Tectonics

RESEARCH ARTICLE
10.1029/2017TC004668

Special Section:
Orogenic cycles: from field observations to global geodynamics

Late Cenozoic Foreland-to-Hinterland Low-Temperature Exhumation History of the Kashmir Himalaya

Yann Gavillot[1], Andrew J. Meigs[1], Francis J. Sousa[1], Daniel Stockli[2,3], Doug Yule[4], and Manzoor Malik[5]

[1]College of Earth, Oceans, and Atmospheric Sciences, Oregon State University, Corvallis, OR, USA, [2]Department of Geology, University of Kansas, Lawrence, KS, USA, [3]Jacksons School of Geosciences, University of Texas at Austin, Austin, TX, USA, [4]Department of Geological Sciences, California State University, Northridge, CA, USA, [5]Department of Geology, University of Jammu, Jammu, India

Abstract New apatite and zircon (U-Th)/He cooling ages quantify late Cenozoic exhumation patterns associated with fault activity across the Kashmir Himalaya. Apatite (U-Th)/He (AHe) cooling ages of detrital grains from the Sub-Himalayan foreland sediments indicate significant resetting. AHe data and thermal modeling reveal cooling and exhumation initiated by 4 Ma at the deformation front and by 2–4 Ma throughout other Sub-Himalayan structures. Exhumation rates for Sub-Himalayan structures are ≥1 mm/year. In the hinterland, thrust sheet samples from the Main Boundary thrust and Main Central thrust yield AHe cooling ages between 5.1 and 21.1 Ma. Published apatite fission track cooling ages (<3 Ma) and high exhumation rates (3.6–3.2 mm/year) across the Kishtwar window further to the north are consistent with AHe data from the Sub-Himalayan structures. The pattern of cooling ages and rates indicates that exhumation occurs in association with changes in the Himalayan basal décollement ramp geometry. Hinterland zircon (U-Th)/He (ZHe) data show a pronounced abundance and probability spike in cooling ages between 14 and 21 Ma, a period when Main Central thrust motion is well documented throughout the Himalaya. ZHe single-grain ages from Sub-Himalayan samples contain a nearly identical cluster from 16 to 23 Ma. Cooling patterns across the Kashmir Himalayas do not correlate spatially with modern monsoon precipitation, suggesting that climate-related precipitation and exhumation are decoupled. Coeval translation over the basal décollement and distributed imbricate thrust deformation of the foreland in the upper plate characterizes fault-related exhumation of the Sub-Himalayan orogenic belt after 4 Ma.

Plain Language Summary Our new data document the timing of cooling of rocks brought to the surface during mountain building of the Kashmir Himalaya. Mineral grains eroded from the Himalaya and deposited in the plain are now exposed in the Sub-Himalayan belt. The ages of these rocks that we have measured constrain the timing of burial and subsequent return to the Earth's surface (exhumation) during thrust fault-related deformation. Analysis of apatite grains reveals that cooling and exhumation initiated by 4 Ma on the southernmost structure of the Kashmir Himalaya and by 2–4 Ma on other distributed faults in the Sub-Himalayan belt. In the core of the mountain range rocks have young cooling ages (<3 Ma) related to high uplift rates within the Kishtwar window, a zone of localized deformation in the High Himalaya. Thus, outward growth of the Sub-Himalayan belt occurred in concert with uplift in the hinterland over the past 4 Myr. Precipitation rates vary systematically from south to north across the Himalaya, but these variations are not synchronous with the pattern of cooling and exhumation in Kashmir Himalaya. This result suggests that climate does not drive crustal deformation. Instead exhumation patterns primarily reflect the location, geometry, and partitioning of faulting within the Himalaya.

Key Points:
- In the Kashmir Himalaya thrust-related cooling and exhumation initiated by 4 Ma at the deformation front and by 2–4 Ma throughout the Sub-Himalayan structures
- A ramp geometry to the Himalayan basal décollement explains across- and along-strike variation in uplift rates and exhumation history
- Distributed deformation between duplex growth in the hinterland and imbricate thrusts in the foreland since 4 Ma suggests a subcritical wedge state

Supporting Information:
- Supporting Information S1

Correspondence to:
Y. Gavillot,
gavilloy@oregonstate.edu

Citation:
Gavillot, Y., Meigs, A. J., Sousa, F. J., Stockli, D., Yule, D., & Malik, M. (2018). Late Cenozoic foreland-to-hinterland low-temperature exhumation history of the Kashmir Himalaya. *Tectonics*, *37*. https://doi.org/10.1029/2017TC004668

Received 25 MAY 2017
Accepted 5 AUG 2018
Accepted article online 17 AUG 2018

1. Introduction

Forward propagating thrust sequences, defined by sequential thrust emplacement from the hinterland to the foreland (e.g., Boyer & Elliott, 1982; Dahlstrom, 1969; Price, 1981; Suppe, 1983), commonly characterize the long-term kinematic evolution of many well-studied mountain belts (i.e., Southern Appalachians, Canadian Rockies, Swiss Alps, Sevier, and others). In detail, however, thrust geometries, syntectonic sediments, major surface-rupturing earthquakes, and other data indicate that orogenic growth occurs via distributed deformation (Boyer & Elliott, 1982; Ji et al., 2001; Jordan et al., 1993; Kaneda et al., 2008; Lee et al., 2001; Meigs & Burbank, 1997; Morley, 1988; Norris & Cooper, 1997). Thus, an emerging image for fold-thrust

belts is that active thrusting varies temporally and spatially and is distributed throughout an orogenic wedge at any given time.

The Himalaya is characterized by a series of south verging thrust splays that branch from the Himalayan basal décollement, the Main Himalayan thrust (MHT; e.g., DeCelles et al., 1998; Lavé & Avouac, 2000; Avouac, 2003). An overall south verging forward propagating thrust sequence is reflected by sequential emplacement at ~22–20 Ma for the Main Central thrust (MCT; Metcalfe, 1993; DeCelles et al., 1998) and after ~11–10 Ma for the Main Boundary thrust (MBT; Meigs et al., 1995, Burbank et al., 1996; Sangode & Kumar, 2003). Paleomagnetic and sedimentological data suggest that onset of thrust-related folding on the Main Frontal thrust or Himalayan Frontal thrust (HFT) at the active deformation front occurred after 2 Ma (Burbank et al., 1996; Kumar et al., 2006; Lavé et al., 2005; Mugnier et al., 1999; Ranga Rao et al., 1988; Sangode & Kumar, 2003; Sapkota et al., 2013; Valdiya, 1998). In Nepal, thermochronological data argue for initiation of thrust-related exhumation at ~2 Ma (van der Beek et al., 2006). In Nepal as well, the HFT shortening rate equals that portion of the India-Asia plate convergence absorbed in the Himalaya (e.g., Bilham et al., 1997; Lavé & Avouac, 2000; Lavé et al., 2005; Mugnier et al., 2004; Sapkota et al., 2013). It is still debated whether active thrusting occurs within the orogenic wedge.

Two competing interpretations of cooling ages, erosion rates, stream gradient indices, and landscape morphology argue for and against active shortening north of the thrust front within the Nepal Himalaya orogenic wedge. The extent to which persistent out-of-sequence thrusting contributes to active and long-term shortening is a central question in the unresolved debate about climatic versus tectonic control of the patterns of deformation within the thrust belt. Correlation of young bedrock cooling ages, high basin-averaged erosion rates, and steep channel gradients in the region of enhanced orographic precipitation on the southern edge of the High Himalaya are interpreted by some workers as evidence of erosional forcing on the pattern of active deformation with out-of-sequence thrusting near the MCT or MBT in the Himalayan hinterland (e.g., Deeken et al., 2011; Hodges et al., 2004; Thiede et al., 2004, 2005, 2009; 2018; Wobus et al., 2003; Wobus et al., 2005; Wobus et al., 2006). In contrast, a number of other arguments using similar data sets favor persistent in-sequence distribution of shortening or that out-of-sequence thrusting is not necessary. Young bedrock cooling ages north of the orographic gradient, balance between geodetic and geologic shortening rates across the thrust front, and thermal-kinematic models argue for orographic precipitation being decoupled from exhumation and/or erosion rates (Blythe et al., 2007; Burbank et al., 2003; Patel & Carter, 2009), and that fault geometry and crustal underplating along the basal décollement (the MHT) control or equally reproduce the cooling pattern and present morphology within the interior of the Himalayan orogen (Bollinger et al., 2006; Brewer & Burbank, 2006; Herman et al., 2010; Robert et al., 2009; van der Beek et al., 2016; Whipp et al., 2007).

Historic surface rupturing earthquakes and folded and faulted Quaternary fluvial terraces provide unequivocal evidence that distributed coeval thrusting across the Sub-Himalaya characterizes active deformation in Kashmir at the western end of the Himalayan orogen (Avouac et al., 2006; Gavillot, 2014; Gavillot et al., 2016; A. Hussain & Yeats, 2009; Vassallo et al., 2015; Vignon, 2011). In this paper we use a new suite of low-temperature thermochronologic data to address the question of whether the active pattern of distributed deformation in the Kashmir Himalaya has persisted over geological timescales $>10^6$ years. New data presented here include detrital samples from sediment exposed by thrust sheets in the foreland of the Sub-Himalaya and in the hinterland of the Pir Panjal Range (Figure 1). Our data set comprises ages from 15 apatite (AHe) and 15 zircon (ZHe) samples, totaling 74 individual single-grain analyses. These data provide the first evidence of reset detrital cooling ages of foreland sediments in the Kashmir or western Himalaya. By combining new data and modeling with previously published data from neighboring areas and a crustal-scale balanced cross section, we provide new constraints on the linkages between exhumation and thrust belt kinematics between the High Himalaya and the Sub-Himalayan foreland of the western Himalaya. In addition, we assess the relative degree of coupling or decoupling between climate and tectonic forcing on the exhumation pattern across the Kashmir Himalaya.

2. Architecture of the Kashmir Himalaya

The Kashmir Himalaya, defined as the region between the Ravi River in India and the Jhelum River in Pakistan, differs in its structural architecture when compared to the central and western Himalaya. The northern fringe

10.1029/2017TC004668

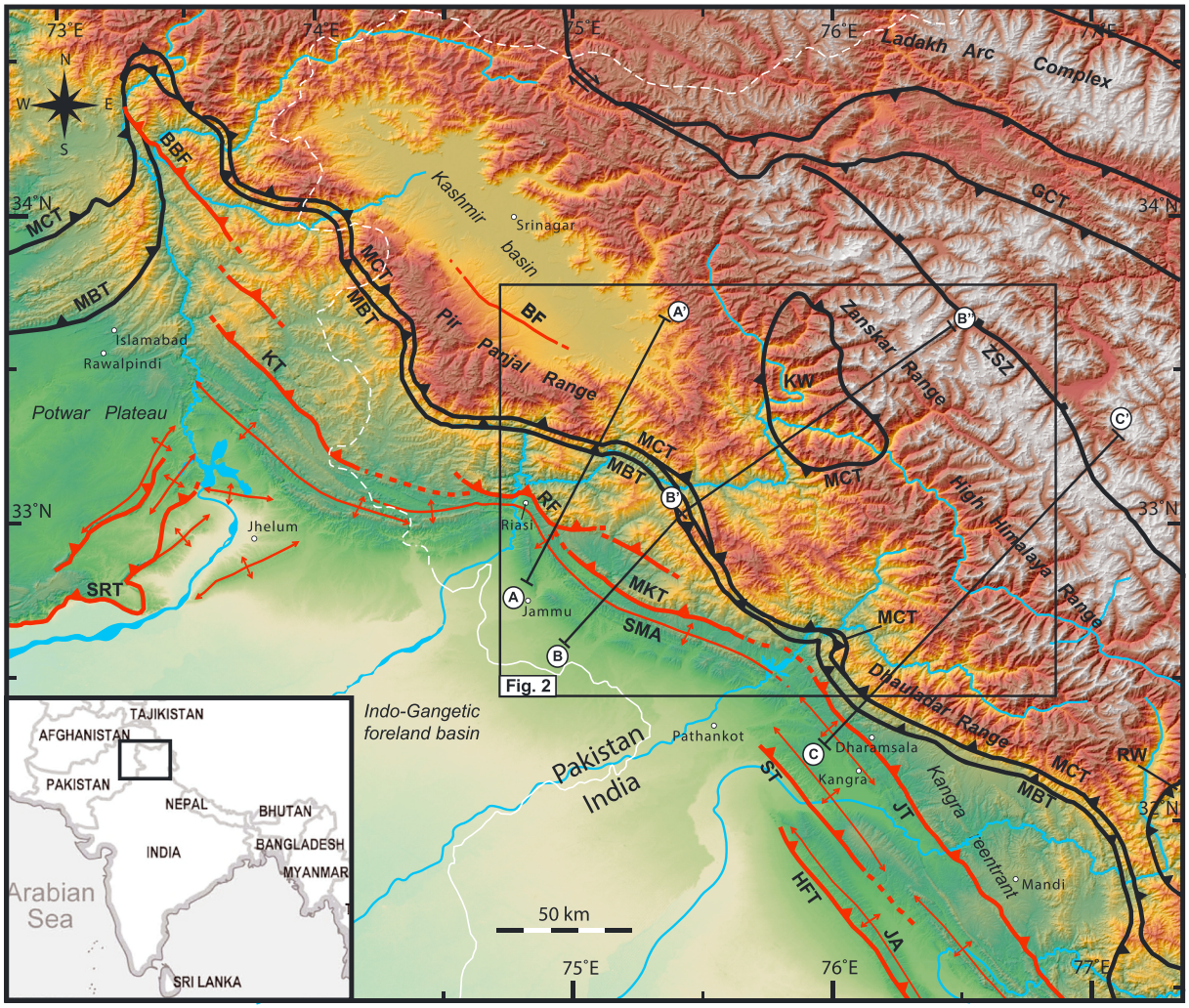

Figure 1. Regional structure map of the Himalaya thrust belt in northwest India and Pakistan. Inset at lower left shows map location. The box shows location of Figure 2. Cross section lines A-A′ and B-B′-B″ are shown in Figure 3. Cross section line C-C′ from Deeken et al. (2011). GCT: Great Counter thrust system; ZSZ: Zanskar shear zone; KW: Kishtwar window; RW: Rampur window; MCT: Main Central thrust; MBT: Main Boundary thrust; BF: Balapora fault; BBF: Balakot-Bagh fault; KT: Kotli thrust; RF: Riasi fault system; MKT: Mandili-Kishanpur thrust; JT: Jawalmukhi thrust; ST: Soan thrust; JA: Janauri anticline; HFT: Himalayan Frontal thrust; SMA: Suruin-Mastgarh anticline; Salt Range thrust.

of the foreland basin, the Sub-Himalayan belt, consists of thick Oligocene-Pliocene foreland basin deposits of the Murree and Siwalik Formations (Figure 2; Hodges, 2000; DiPietro & Pogue, 2004). Map relations, regional cross sections (lines A-A′ and B-B″ in Figure 3), and published data indicate stratigraphic thicknesses of 2–3.6 km for the Murree Formation and ~6 km for the Siwalik Formation (Karunakaran & Ranga Rao, 1976; Powers et al., 1998; Shah, 2009; Thakur, 1992; Thakur & Rawat, 1992). Active shortening is distributed between the Suruin-Mastgarh anticline (SMA) at the deformation front and on faults to the north within the Sub-Himalaya (Figure 2; Kaneda et al., 2008; Kondo et al., 2008; Gavillot, 2014; Gavillot et al., 2010; Gavillot et al., 2016; A. Hussain & Yeats, 2009; Thakur et al., 2010).

The SMA is a symmetric fold that defines the deformation front in Kashmir (Figure 2). In contrast to the HFT of the central and western Himalaya, the SMA is not bound by a foreland-directed emergent thrust fault, and neither of its limbs is cut by a fault at the surface. Active emergent thrust faulting within the Sub-Himalaya, rather, occurs roughly 40 km north of the deformation front, on the Riasi fault system (RF) and its along-strike correlative the Mandili-Kishanpur thrust (MKT; Ranga Rao & Datta, 1976; Raiverman et al., 1983). Further to the north, other faults that deform the subHimalaya include the Tanhal (TT) and Mundun thrusts (MT). The RF in the Kashmir Himalaya has structural and stratigraphic similarities with a series of en-echelon faults to the northwest in neighboring Pakistan Azad Kashmir, which include the Kotli thrust (KT) and the Balakot-Bagh

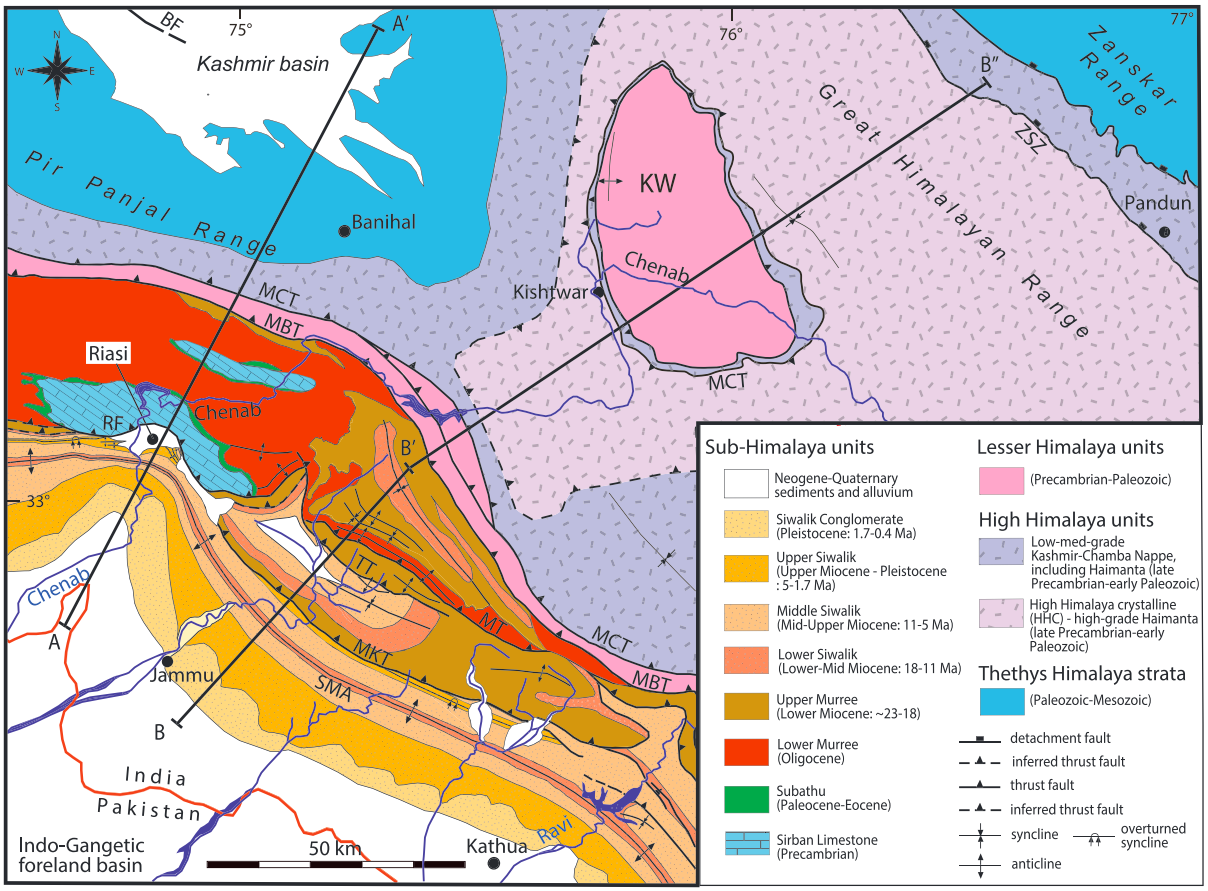

Figure 2. Regional geologic map of the Kashmir Himalaya (modified after Ranga Rao & Datta, 1976; Raiverman et al., 1983; Thakur & Rawat, 1992; and DiPietro & Pogue, 2004). ZSZ: Zanskar shear zone; KW: Kishtwar window; MCT: Main Central thrust; MBT: Main Boundary thrust; BF: Balapora fault; RF: Riasi fault system; MT: Mundun thrust; TT: Tanhal thrust; MKT: Mandili-Kishanpur thrust; SMA: Suruin-Mastgarh anticline. See Figure 3 for cross sections.

fault (BBF; Figure 1; Ranga Rao & Datta, 1976; Iqbal et al., 2004; S. Hussain et al., 2004). Evidence that the RF, KT, and BBF are genetically linked includes the faults' position within the orogenic belt behind the deformation front and unique hanging wall stratigraphic successions marked by 5-km-thick Precambrian limestone (Sirban Limestone Formation in India) and Paleocene-Eocene limestone (Subathu Formation in India; Figures 2 and 3; Ranga Rao & Datta, 1976; Thakur, 1992; Thakur & Rawat, 1992; S. Hussain et al., 2004; Iqbal et al., 2004; A. Hussain & Yeats, 2009). Together, the RF, KT, and BBF represent a seismically active emergent thrust fault system that extends stepwise more than 200 km northwestward along strike within the orogenic wedge (A. Hussain & Yeats, 2009; MonaLisa, 2009; Gavillot et al., 2016). Published estimates of Pleistocene-Holocene shortening rates across Sub-Himalayan foreland structures include $<$6 to 9 mm/year for the SMA, 6 to 7 mm/year for the RF, and ~3 mm/year for the BBF (Gavillot, 2014; Gavillot et al., 2016; Gavillot, Axen, et al., 2010; Kondo et al., 2008; Vassallo et al., 2015; Vignon, 2011).

In the hinterland, the MBT and MCT, locally known as the Murree and Panjal thrusts, respectively (Thakur, 1992; Thakur & Rawat, 1992; Wadia, 1934), form a narrow, $<$10-km-wide zone along the southern flank of the Pir Panjal Range (Figures 1 and 2). The MBT bounds the Lesser Himalaya units and carries the Ramban Formation, a Proterozoic-aged sequence of low-grade slate and phylitte (Bhatia & Bhatia, 1973; Thakur, 1992; Thakur & Rawat, 1992; Wadia, 1934). These metamorphic rocks are the same age as or younger than the Precambrian Sirban Limestone (Thakur, 1992; Thakur & Rawat, 1992). North of the MCT, a series of nappes and highly deformed metamorphic rocks of the High Himalaya units, which include the low-grade Haimanta Group and the high-grade High Himalaya Crystalline of late Precambrian to early Paleozoic age (Bhatia & Bhatia, 1973; Frank et al., 1995; Griesbach, 1891; Searle et al., 2007; Thakur, 1992; Thakur, 1998; Thakur & Rawat, 1992 and references therein). At the Kishtwar window (KW), a 45-km-wide structural culmination

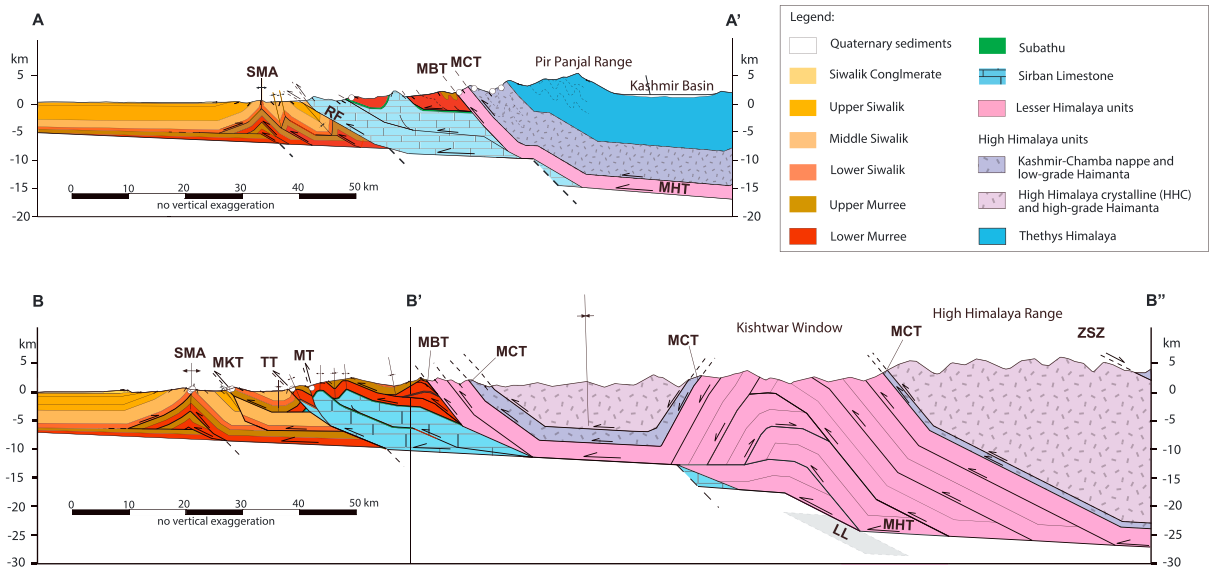

Figure 3. SW-NE regional cross sections across the Kashmir Himalaya along the lines A-A′ and B-B′-B″. See Figure 2 for locations. The white circles represent sample locations for new AHe age data. Section line A-A′ depicts structural interpretation along the longitude of the Chenab reentrant and Riasi fault system (RF; after Gavillot et al., 2016). Section line B-B′ is structural interpretation along strike to the southeast, crossing the deformation front (SMA), Sub-Himalayan thrusts (Mandili-Kishanpur thrust [MKT], Tanhal thrust [TT], and Mundun thrust [MT]), and northward to the Kishtwar window (KW) and Zanskar Shear Zone (ZSZ) in the hinterland. Structural interpretation across the Kishtwar window in section line B′-B′-B″ is constrained by balanced cross sections, shown in Figure 10. Style of deformation across Kishtwar window is inspired from previously published cross sections after DiPietro and Pogue (2004), Yin (2006), and Searle et al. (2007). LL: Projected location of interseismic locking line after Schiffman et al. (2013). Fault name abbreviations listed in Figure 2.

exposing Lesser Himalayan units is interpreted to be an antiformal stack duplex (Figures 2 and 3; DiPietro & Pogue, 2004; Yin, 2006; Searle et al., 2007). The MHT acts as the basal décollement and the MCT represents the roof thrust of the KW duplex. Rocks from within the KW thus represent structurally deeper levels than rocks above the MCT (Figure 3). At the northern end of the Kashmir High Himalaya, the Zanskar Range is bounded by the Zanskar Shear Zone (ZSZ) carrying Tethys Himalaya strata (Figures 2 and 3), which correlate to the South Tibetan Detachment fault (DiPietro & Pogue, 2004; Searle et al., 2007; Searle & Godin, 2003; Yin, 2006).

3. Apatite and Zircon (U-Th)/He Thermochronometry

3.1. Background and Analytical Methods

^{4}He ingrowth in apatite and zircon occurs primarily due to alpha decays in the ^{235}U, ^{238}U, and ^{232}Th decay chains. These (U-Th)/He thermochronometers are of particular value to the study of tectonic processes because of their low closure temperatures (40–80 °C for AHe, 140–220 °C for ZHe). Detailed studies over the last several decades have significantly enhanced understanding of He diffusion in natural apatite and zircon minerals on geologic timescales (e.g., Farley & Stockli, 2002; Flowers et al., 2009; Guenthner et al., 2013; Reiners, 2005; Reiners et al., 2004).

The temperature range over which apatite grains in natural samples transition from total diffusive loss to quantitative retention of He is the AHe Partial Retention Zone, AHePRZ (e.g., Farley & Stockli, 2002; Wolf et al., 1998). The limits of the AHePRZ generally range from 40 to 80 °C, which depends on variability in grain size, cooling rate, and effective Uranium (eU) concentration (Farley & Stockli, 2002; Flowers et al., 2009). The higher closure temperature for ZHe corresponds to a hotter ZHePRZ, and variations among individual grains can have a strong effect on closure temperature (e.g., Guenthner et al., 2013; Reiners, 2005; Reiners et al., 2004). Generally, the ZHePRZ spans a temperature range from 120 to 220 °C (Guenthner et al., 2013; Stockli, 2005; Tagami et al., 2003). Another widely used low-temperature thermochronometer is fission track (FT) dating. FTs are linear zones of damage that result from the spontaneous fission of 238U within the crystal lattice that are retained at temperatures lower than that of the *partial annealing zone* (PAZ; e.g., Gleadow & Fitzgerald, 1987). In a setting of fault-related cooling and exhumation, apatite fission track (AFT) and apatite He (AHe) data typically show related cooling histories, given that the AFT system has a slighter higher closure temperature of 60–110 °C and apatite PAZ of 70–120 °C (Gleadow & Fitzgerald, 1987; Ketcham et al., 1999)

than the He closure temperature and apatite HePRZ (40–80 °C). Zircon fission track (ZFT) ages record cooling below the ~240 °C closure temperature, and the zircon PAZ spans 250–350 °C (Bernet & Spiegel, 2004; Cerveny et al., 1988; Rahn et al., 2004; Tagami et al., 1996, 1998; Tagami & Dumitru, 1996).

Apatite or zircon grains from sedimentary rocks that have been reheated to sufficient temperatures yield reset detrital cooling ages. For a given thermochronometer, a cooling age is reset when the sample reaches sufficient stratigraphic or structural overburden dependent on the geothermal gradient and shape of the subsurface isotherms. Because of its low closure temperature, the AHe system is sensitive to relatively shallow crustal levels of exhumation and cooling. This sensitivity demonstrates the potential of AHe data to constrain activity of individual faults under suitable settings in fault geometry, displacement rates, and geothermal gradient (Ehlers & Farley, 2003; Flowers et al., 2009; Gavillot et al., 2010; Sousa et al., 2016). Tectonically driven exhumation in the upper plate of a thrust sheet as recorded by He or FT data may result from fault displacement or from passive uplift forced by structurally deeper thrust faults (Bollinger et al., 2006; Gavillot, Meigs, et al., 2010; Robert et al., 2009; Whipp et al., 2007).

Individual AHe and ZHe ages were measured from 11 sedimentary samples and 4 metamorphic samples in the study area. After standard heavy liquids separation, individual apatite and zircon grains were selected for analyses based on grain size, euhedral morphology, and lack of visible inclusions when examined under a stereoscopic microscope. Based on these criteria, AHe and ZHe dates were determined on three to five of the highest quality grains per sample. For more detailed descriptions of the analytical technique, see Stockli et al., 2000, Farley and Stockli (2002), Ehlers and Farley (2003), and Stockli (2005). Concentrations of ^{4}He, U, Th, and Sm were measured by isotope dilution using a quadrupole mass spectrometer (for ^{4}He) and inductively couple plasma mass spectrometer (for U, Th, and Sm) at the University of Kansas U-Th/He Lab (now at the University of Texas, Austin).

Mean AHe and ZHe ages were calculated on the basis of replicate single-grain analyses, with uncertainties reported as standard error of the mean. For most samples three to five single-grain ages were retained to calculate mean ages. Single-grain ages excluded in the mean sample age calculations were identified on the basis of analytical inconsistency in the laboratory measurements (e.g., no measurable He; grains other than apatite measured; inclusions). A few samples with limited replicate single-grain analyses yielded two single grains to calculate mean ages. Analytical uncertainties reported for each single grain analysis (2 sigma) are estimated as 6% for apatite and 8% for zircon.

3.2. Sampling Methods

Field sampling targeted hanging wall and footwall units of various thrust sheets in both the foreland and hinterland to document thrust-related exhumation. In our study we refer to foreland samples as those from the sub-Himalayan belt between the thrust front and the MBT, and hinterland samples as those collected between the MBT and the ZSZ (Figures 2–4). Samples were taken from elevations ranging from 500 to 1,500 m, within drainage basins and on ridges, respectively.

Eleven foreland samples were collected from sedimentary rocks of the Sub-Himalaya belt (Figures 2–4). Sample lithologies include sand and silt-rich intervals from the Oligocene to Early Miocene Murree Formations (IHM-3, IHM-4, IHM-8, IHM-9, IHM-14, IHM-15, and IHM-16) and the Early to Middle Miocene Lower-Middle Siwalik Formations (IHS-1, IHS-5, IHS-6, and IHS-7; Tables 2 and 3). For each sample, roughly 5 kg of sample material was collected in the field.

Four hinterland samples were taken from metamorphic rocks from the Lesser (one sample) and High Himalaya (three samples) along a 15-km-long transect across thrust sheets of the MBT and MCT (Figures 2–4). The Lesser Himalaya sample is from silt-rich phylitte intervals within the flysch-like Precambrian Ramban Formation (IHR-10; Wadia, 1937; Bhatia & Bhatia, 1973; Thakur, 1992; Thakur & Rawat, 1992). The High Himalaya samples come from gneiss, schist, and metavolcanic lithologies (IHSC-11, IHP-12, and IGC-13; Bhatia & Bhatia, 1973; Thakur & Rawat, 1992).

3.3. Thermal History Constraints

We broadly constrain the thermal history of our samples by combining the stratigraphic thicknesses of the Murree and Siwalik Formations with previously published estimates of geothermal gradient. We use a geothermal gradient of 18–24 °C/km for the Sub-Himalayan (after Agarwal et al., 1994; van der Beek et al.,

10.1029/2017TC004668

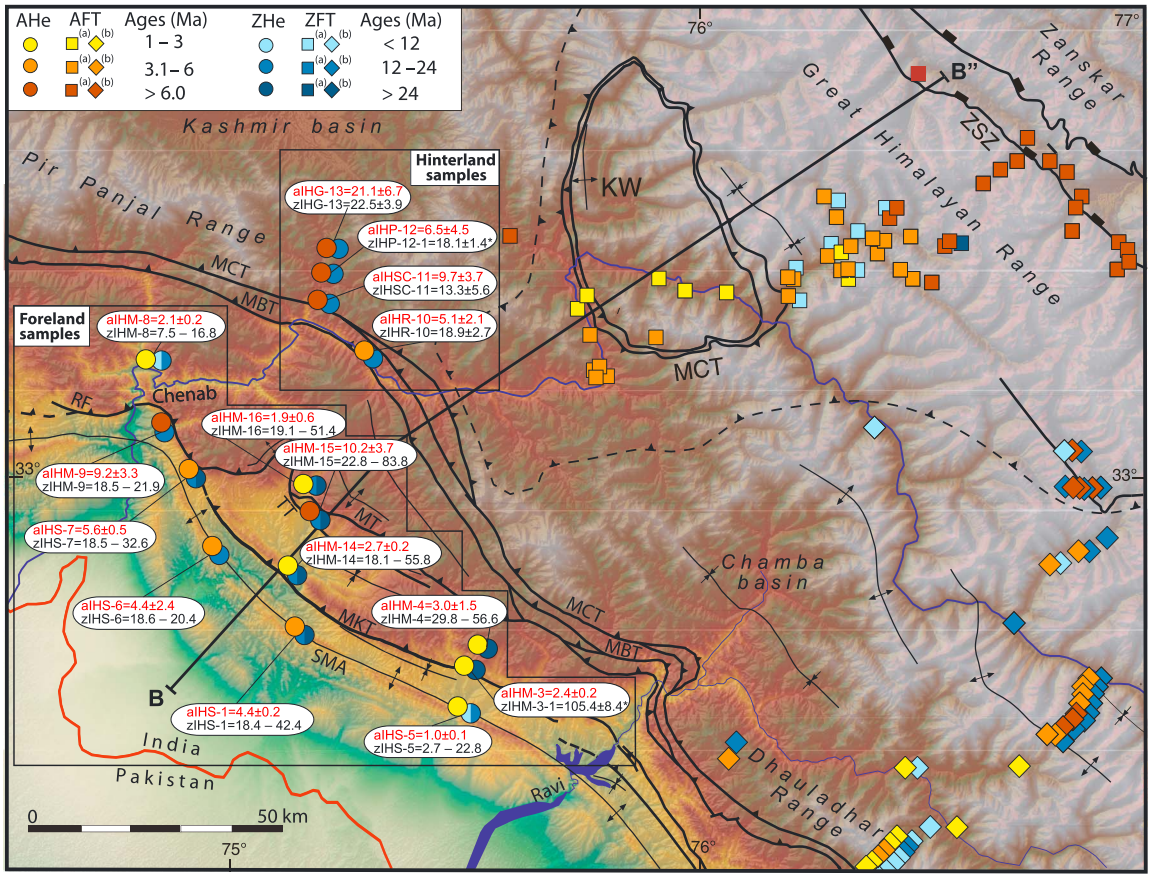

Figure 4. AHe and ZHe regional age distribution map. The circles are data from this study, grouped into hinterland and foreland samples, and indicating respective sample names, as reported in Tables 2 and 3. The star symbol (*) indicates where only a single-grain age analysis is available. The square and diamond symbols denote published AFT and ZFT age data from (a) Kumar et al. (1995) and (b) Deeken et al. (2011). See Figure 11 for data compilation correlated with regional cross section along line B-B′-B″ across the Kashmir Himalaya. Fault name abbreviations listed in Figure 2.

2006) and 30–45 °C for the Pir Panjal and High Himalaya (Deeken et al., 2011; Kumar et al., 1995; Stübner et al., 2018), reflecting thermal differences between thick and cold foreland sediments, and more deeply exhumed crustal rocks in the hinterland. Additionally, we use a mean annual surface temperature of 20 °C for the Sub-Himalaya valleys and 10 °C for the Pir Panjal and High Himalaya Ranges.

Table 1 lists the stratigraphic thickness, cumulative stratigraphic overburden, and paleotemperature estimates of the foreland samples. Thicknesses are constrained from map relations, published measured sections, structural data, and cross sections (Figures 2 and 3). In locations where the units are not well exposed, stratigraphic thicknesses are constrained by our cross sections as well as data from previous studies (Karunakaran & Ranga Rao, 1976; Powers et al., 1998; Thakur & Rawat, 1992). Measurements of overburden for the foreland samples include units between the Lower Murree (34 to 23 Ma) and at minimum the basal section of the Upper Siwalik Formation (5 to 1.7 Ma), because structural disruption by thrusts in the Sub-Himalaya belt is presumed to have been underway during Upper Siwalik deposition (Burbank et al., 1996; Kumar et al., 2006; Mugnier et al., 1999; Ranga Rao et al., 1988; Sangode & Kumar, 2003; Valdiya, 1998; van der Beek et al., 2006).

Overburden at the deformation front, along the core of the SMA is estimated to have a stratigraphic thickness of 3.1–4.6 km for the base of Lower Siwalik Formation and 2.5–3.4 km for the base of the Middle Siwalik Formation. For our assumed geothermal gradients and average surface temperature, the thickness of overburden translates to prethrust burial temperatures ranging from 75 to 127 °C for the Lower Siwalik and 65 to 102 °C for the Middle Siwalik (Table 1). Overburden for the deeper stratigraphic levels along the Sub-Himalayan thrust sheets is estimated to be 5.8–7.8 km for the base of the Lower Murree and 4.0–5.8 km for

Table 1
Stratigraphic Thickness, Overburden, and Paleotemperature for Kashmir Foreland Strata

Stratigraphic unit and age	Thickness (m) in transect A-A′	Thickness (m) in transect B-B″	Total range (m)	Stratigraphic overburden (m)	Min paleotemp (°C)	Max paleotemp (°C)	Total range (°C)
Upper Siwalik (5–1.7 Ma)	3,000	3,300	3,000–3,300	–	–	–	–
Middle Siwalik (11–5 Ma)	1,500–1,800	2,100–2,400	1,500–2,400	2,500–3,400 (b) (IHS-7)	65–81	80–102	65–102
Lower Siwalik (18–11 Ma)	560–670	890–1,050	560–1,050	2,780–3,925 (m) (IHS-1/5)	70–91	87–114	70–114
				3,060–4,550 (b) (IHS-6)	75–100	93–127	75–127
Upper Murree (23–18 Ma)	890	1,300	890–1,300	3,060–4,450 (t) (IHM-9/15)	75–100	93–127	75–127
				3,950–5,750 (b) (IHM-3/4/14)	91–124	115–158	91–158
Lower Murree (34–23 Ma)	2,000	1,800	1,800–2,000	4,850–6,750 (m) (IHM-16)	107–142	136–182	107–182
				5,750–7,750 (b) (IHM-8)	124–160	158–206	124–206

Note. Thickness estimates for two different areas correlating with cross sections lines A-A′ (Chenab reentrant) and B-B′ (Jammu-Udhampur area). Siwalik unit thicknesses derived from cross-section constraints and estimates taken from published studies (Karunakaran & Ranga Rao, 1976; Powers et al., 1998). See Figure 2 for location. Paleotemperatures are calculated using ~20 °C average surface temperature for the Sub-Himalaya and range of geothermal gradients between a minimum (18 °C/km) and maximum (24 °C/km) taken from published literature for the Sub-Himalaya in India (Agarwal et al., 1994) and Nepal (Van der Beek et al., 2006). Stratigraphic overburden estimates are derived from range of values from both transect areas (Chenab reentrant and Jammu-Udhampur) for a given sample (e.g., IHM-8) within the basal (b), middle (m), or top (t) section of a unit (see Tables 1 and 2). Minimum contribution of stratigraphic overburden from 3,000- to 3,300-m-thick Upper Siwalik Formation (5–1.7 Ma) is limited to the lower part, estimated to be at minimum ~1,000-m-thick, because structural disruption by thrusts in the Sub-Himalaya belt was underway and while these deposits accumulated.

the base of the Upper Murree, suggesting burial temperatures ranging from 124 to 206 °C and 91 to 158 °C, respectively (Table 1).

These estimates indicate that all of the units except the Upper Siwalik Formation potentially reached temperatures hot enough to significantly reset AHe ages. In contrast, only the deepest part of the Murree Formations was heated to sufficient temperatures to reset ZHe ages.

Based on thrust sheet and stratigraphic thicknesses of the Kashmir Tethys Himalaya strata, we estimate the overburden of the rocks sampled from the Lesser Himalaya and High Himalaya to be at minimum ~8 km (Thakur & Rawat, 1992), which excludes likely overburden from the Murree Formations or equivalent foreland sediments prior to being eroded off during hinterland exhumation. Assuming a higher hinterland geothermal gradient of 30–45 °C for deeper crustal exhumation of the Lesser and High Himalaya metamorphic rocks (Deeken et al., 2011; Kumar et al., 1995; Stübner et al., 2018) translates to minimum burial paleotemperatures ranging from 280 to 360 °C, hot enough to fully reset AHe and ZHe ages.

3.4. Thermal Modeling Methods

In order to better constrain the sample thermal histories beyond these general estimates based on stratigraphic thickness, we utilize the thermochronologic modeling software, QTQt, to extract quantitative thermal history information from the AHe data (Flowers et al., 2015; Gallagher, 2012; Vermeesch & Tian, 2014). QTQt employs a trans-dimensional Bayesian Monte Carlo Markov chain (MCMC) statistical approach to find the best time-temperature (t-T) paths for a sample by employing a large number of iterative perturbations (we use at least 10^6 iterations). After each perturbation, the model compares the initial path to the proposed path and chooses the better of the two according to an acceptance criterion (Gallagher, 2012). During the *burn-in* period, the model converges on the best fit t-T path (Gallagher, 2012). For each of our model runs the burn-in period consists of at least 5×10^5 iterations (Sousa et al., 2016, 2017; Vermeesch & Tian, 2014). After the model has converged on a best fit t-T path, we run an additional set of 5×10^5 *post–burn-in* iterations to document the distribution of best fit t-T histories. The model outputs show the results of this post–burn-in period. The RDAAM model of Flowers et al. (2009) is utilized directly in QTQT for all model runs reported here to account for variable kinetic behavior.

We also impose a minimal set of manually controlled thermal history constraints. For each detrital sample we impose a low-temperature constraint of 15–20 °C at some point during the time of deposition (Table 2). We

Table 2
Thermal History Model Input Table

Sample num.	Model runs	Time-temperature bounding box	Low-temperature constraints	Modern-temperature constraints	No. of pre–*burn-in* iterations	No. of post–burn-in iterations
IHS-1	Three apatite grains[a]	50 Ma 0 Ma 85° ± 70°	18–11 Ma 17.5° ± 2.5°	20° ± 5°	≥500,000	500,000
IHS-5	Four apatite grains[a]	50–0 Ma 85° ± 70°	23–18 Ma 17.5° ± 2.5°	20° ± 5°	≥500,000	500,000
IHS-6	Three apatite grains[a]	50–0 Ma 85° ± 70°	18–11 Ma 17.5° ± 2.5°	20° ± 5°	≥500,000	500,000
IHM-3	Three apatite grains[a]	50–0 Ma 85° ± 70°	18–11 Ma 17.5° ± 2.5°	20° ± 5°	≥500,000	500,000
IHM-4	Three apatite grains[a]	50–0 Ma 85° ± 70°	18–11 Ma 17.5° ± 2.5°	20° ± 5°	≥500,000	500,000
IHM-14	Four apatite grains[a]	50–0 Ma 85° ± 70°	18 Ma – 11 Ma 17.5° ± 2.5°	20° ± 5°	≥500,000	500,000
IHS-7	Four apatite grains[a]	60–0 Ma 85° ± 70°	11–5 Ma 17.5° ± 2.5°	20° ± 5°	≥500,000	500,000
IHM-8	Four apatite grains[a]	50–0 Ma 85° ± 70°	34–23 Ma 17.5° ± 2.5°	20° ± 5°	≥500,000	500,000
IHM-9	Four apatite grains[a]	50–0 Ma 85° ± 70°	23–18 Ma 17.5° ± 2.5°	20° ± 5°	≥500,000	500,000
IHM-15	Four apatite grains[a]	60–0 Ma 85° ± 70°	23–18 Ma 17.5° ± 2.5°	20° ± 5°	≥500,000	500,000
IHM-16	Three apatite grains[a]	60–0 Ma 85° ± 70°	34–23 Ma 17.5° ± 2.5°	20° ± 5°	≥500,000	500,000
IHR-10	Two apatite grain average[b] Three zircon grain average[b]	70–0 Ma 150° ± 145°	none none	10° ± 5°	≥500,000	500,000
IHSC-11	Two apatite grain average[b] Three zircon grain average[b]	70–0 Ma 150° ± 145°	none none	10° ± 5°	≥500,000	500,000

[a]One model run per individual grain. [b]One model run per sample.

use a reasonable bounding box of temperature and time for the model to explore different possible cooling paths (80 ± 75 °C, 50 or 60 Ma to present), and a rough estimate of modern mean annual surface temperature 20 ± 5 °C as a present-day temperature constraint. For the Sub-Himalayan foreland sedimentary samples, we present a separate model for each single grain detrital AHe age. To extract information from potentially reset ZHe data, we also modeled a limited set of single ZHe dates (supporting information S1). For the hinterland metamorphic bedrock samples we ran a single aggregate model based on the sample average AHe and ZHe data, with a bounding box of 150 ± 135 °C, 70 Ma to present, and no low-temperature depositional constraint (Table 2 and supporting information S1).

4. Results

4.1. AHe Data

4.1.1. Foreland Samples

Foreland samples were collected across the fold axis and limbs of the SMA and across the thrust sheets of the MKT, RF, TT, and MT from south to north, respectively (Figure 4). At the deformation front, three samples, IHS-1, IHS-5, IHS-6, from the Lower Siwalik Formation along the core of the SMA yield AHe mean sample ages of 4.4 ± 0.2, 1.0 ± 0.1 Ma, and 4.4 ± 2.4 Ma, respectively (Figure 4, Table 3, and supporting information S2), all younger than the Siwalik strata from which they were sampled (Figure 5a).

In the MKT thrust sheet, three samples from the Upper Murree Formation yield broadly consistent mean AHe ages of 2.4 ± 0.2 Ma (IHM-3), 3.0 ± 1.5 Ma (IHM-4), and 2.7 ± 0.3 Ma (IHM-14; Figure 4, Table 3, and supporting information S2). Samples from the northeastern limb of the SMA and the RF footwall are from the Middle Siwalik (IHS-7) and Upper Murree Formations (IHM-9; Figure 4). Mean ages of the two samples are 5.6 ± 0.5 Ma and 9.2 ± 3.3 Ma, respectively. The RF hanging wall sample (IHM-8) from the Lower Murree Formation is younger than the footwall samples, with a mean age of 2.1 ± 0.2 Ma (Figure 4, Table 3, and

Table 3
Kashmir Himalaya Apatite (U-Th)/He Data for Both Single-Grain and Mean Sample Ages

Sample num.	Age (Ma)	± (Ma)	U (ppm)	Th (ppm)	147Sm (ppm)	e (U)	Th/U	He (nmol/g)	Mass (ug)	Ft	ESR	Standard error of mean
Suruin-Mastgarh anticline (SMA)												
IHS-1-1	4.5	0.27	58.4	4.6	105.6	60.0	0.08	0.93	1.50	0.64	38.85	
IHS-1-2	4.5	0.27	40.5	4.2	68.0	41.8	0.10	0.75	3.52	0.72	52.35	
IHS-1-3	4.2	0.25	17.3	3.8	52.5	18.5	0.22	0.33	6.49	0.77	63.27	
IHS-1	**4.4**	**0.3**	**38.7**	**4.2**	**75.3**	**40.1**	**0.1**	**0.67**	**3.8**	**0.7**	**51.5**	**0.17**
IHS-5-1	1.0	0.06	5.8	2.4	31.3	6.5	0.42	0.02	2.53	0.69	46.94	
IHS-5-2	1.1	0.07	4.0	3.3	25.4	4.9	0.82	0.02	3.31	0.71	51.86	
IHS-5-3	0.9	0.06	6.3	2.9	35.2	7.1	0.47	0.03	2.85	0.70	49.53	
IHS-5-4[a]	9.7	0.58	8.9	6.8	38.7	10.6	0.77	0.38	2.04	0.66	44.14	
IHS-5	**1.0**	**0.1**	**5.3**	**2.9**	**30.6**	**6.2**	**0.6**	**0.02**	**2.9**	**0.7**	**49.4**	**0.11**
IHS-6-1	2.8	0.17	10.3	3.8	10.5	11.2	0.37	0.12	3.70	0.72	53.68	
IHS-6-2	7.1	0.42	79.7	18.5	29.3	84.1	0.23	1.98	1.25	0.62	36.67	
IHS-6-3	3.3	0.20	1.5	1.7	5.9	1.9	1.13	0.02	2.48	0.67	46.12	
IHS-6	**4.4**	**0.2**	**24.2**	**6.7**	**19.1**	**25.8**	**0.6**	**0.54**	**2.6**	**0.7**	**46.5**	**2.35**
Mandili-Kishanpur thrust (MKT)												
IHM-3-1	2.6	0.15	43.9	429.6	138.0	143.5	9.78	0.64	0.17	0.31	19.62	
IHM-3-2[a]	−17.7	−1.06	4.1	20.7	21.4	9.0	5.02	−0.28	0.22	0.32	19.82	
IHM-3-3[a]	12.6	0.76	2.9	23.0	38.7	8.4	7.95	0.31	0.68	0.52	30.88	
IHM-3-4	2.3	0.14	32.6	146.9	103.5	66.9	4.51	0.30	0.23	0.35	21.06	
IHM-3	**2.4**	**0.1**	**38.2**	**288.2**	**120.7**	**105.2**	**7.1**	**0.47**	**0.2**	**0.3**	**20.3**	**0.17**
IHM-4-1[a]	163.3	9.80	2.4	67.0	65.1	18.1	28.34	9.05	0.83	0.54	33.45	
IHM-4-2	4.1	0.24	13.5	74.2	63.9	30.9	5.49	0.45	2.29	0.65	45.17	
IHM-4-3[a]	17.8	1.07	44.3	135.5	113.7	76.1	3.06	4.82	2.39	0.65	43.88	
IHM-4-4	1.9	0.11	28.0	138.8	77.1	60.4	4.95	0.38	1.38	0.61	39.55	
IHM-4	**3.0**	**0.2**	**20.8**	**106.5**	**70.5**	**45.6**	**5.2**	**0.42**	**1.8**	**0.6**	**42.4**	**1.53**
IHM-14–1	3.0	0.18	29.5	383.7	92.7	118.3	13.01	1.23	1.54	0.62	41.12	
IHM-14-2	2.7	0.16	36.3	305.0	72.0	106.9	8.40	1.03	2.10	0.66	45.70	
IHM-14-3	2.7	0.16	15.7	193.0	46.3	60.3	12.32	0.57	2.19	0.64	44.25	
IHM-14-4	2.4	0.15	50.2	485.3	83.3	162.3	9.67	1.49	3.41	0.69	51.01	
IHM-14	**2.7**	**0.2**	**32.9**	**341.8**	**73.6**	**112.0**	**10.9**	**1.08**	**2.3**	**0.7**	**45.5**	**0.25**
Riasi fault system (RF)												
IHS-7-1	6.0	0.36	60.5	7.7	48.7	62.5	0.13	1.48	4.08	0.74	54.85	
IHS-7-2	5.3	0.32	38.5	7.7	64.8	40.6	0.20	0.82	2.70	0.70	48.62	
IHS-7-3[a]	10.5	0.63	3.4	7.9	36.2	5.4	2.33	0.22	3.27	0.70	51.24	
IHS-7-4[a]	39.5	2.37	17.9	18.6	27.3	22.3	1.04	3.18	2.61	0.66	44.44	
IHS-7	**5.6**	**0.34**	**49.5**	**7.7**	**56.8**	**51.6**	**0.2**	**1.15**	**3.4**	**0.7**	**51.7**	**0.48**
IHM-8-1	2.1	0.13	12.2	23.2	63.8	17.9	1.89	0.14	3.14	0.70	51.09	
IHM-8-2	2.0	0.12	13.4	8.9	40.9	15.7	0.67	0.12	3.06	0.70	50.08	
IHM-8-3	1.9	0.12	11.2	36.2	30.7	19.7	3.24	0.14	1.95	0.65	44.17	
IHM-8-4	2.3	0.14	19.4	32.0	52.8	27.0	1.65	0.23	2.43	0.67	46.82	
IHM-8	**2.1**	**0.1**	**14.0**	**25.1**	**47.0**	**20.1**	**1.9**	**0.16**	**2.6**	**0.7**	**48.0**	**0.18**
IHM-9-1	10.1	0.60	6.9	4.8	42.1	8.3	0.69	0.29	1.76	0.63	39.23	
IHM-9-2	6.7	0.40	4.5	6.6	10.1	6.1	1.47	0.15	2.35	0.66	44.06	
IHM-9-3	13.6	0.82	30.8	4.9	6.9	31.9	0.16	1.78	5.36	0.76	60.63	
IHM-9-4	6.5	0.39	17.9	7.9	49.3	20.0	0.44	0.52	5.06	0.74	57.14	
IHM-9	**9.2**	**0.6**	**15.0**	**6.0**	**27.1**	**16.6**	**0.7**	**0.68**	**3.6**	**0.7**	**50.3**	**3.34**
Tanhal thrust (TT) and Mundun thrust (MT)												
IHM-15-1	11.0	0.66	4.2	17.9	103.1	8.9	4.23	0.29	0.72	0.52	30.97	
IHM-15-2	6.1	0.37	107.9	198.2	23.0	153.7	1.84	2.69	0.67	0.53	30.50	
IHM-15-3	8.7	0.52	4.3	10.7	5.4	6.8	2.52	0.22	2.75	0.69	50.00	
IHM-15-4	14.8	0.89	4.2	22.4	102.8	9.9	5.32	0.45	0.83	0.54	32.83	
IHM-15	**10.2**	**0.6**	**30.2**	**62.3**	**58.5**	**44.8**	**3.5**	**0.91**	**1.2**	**0.6**	**36.1**	**3.68**
IHM-16-1	1.3	0.08	8.0	212.6	34.8	57.1	26.60	0.29	5.03	0.73	61.43	
IHM-16-2	2.1	0.12	22.5	211.0	112.8	71.6	9.38	0.55	2.83	0.68	49.27	
IHM-16-3	2.4	0.14	34.4	187.2	40.6	77.7	5.44	0.76	5.57	0.74	62.68	
IHM-16	**1.9**	**0.1**	**21.6**	**203.6**	**62.7**	**68.8**	**13.8**	**0.54**	**4.5**	**0.7**	**57.8**	**0.59**
MBT/MCT (Pir Panjal Range)												
IHR-10-1[a]	4.0	0.24	−1.1	−0.8	−0.5	−1.3	0.69	−0.02	1.78	0.66	43.19	
IHR-10-2	6.6	0.40	9.4	55.7	128.2	22.9	5.89	0.44	0.68	0.53	31.31	
IHR-10-3	3.6	0.22	7.6	122.3	88.2	36.2	16.00	0.42	1.37	0.59	37.41	

Table 3 *(continued)*

Sample num.	Age (Ma)	± (Ma)	U (ppm)	Th (ppm)	147Sm (ppm)	e (U)	Th/U	He (nmol/g)	Mass (ug)	Ft	ESR	Standard error of mean
IHR-10	**5.1**	**0.3**	**8.5**	**89.0**	**108.2**	**29.6**	**10.9**	**0.43**	**1.0**	**0.6**	**34.4**	**2.13**
IHSC-11-H-1	12.3	0.74	19.3	3.9	22.9	20.3	0.20	0.92	2.17	0.68	44.92	
IHSC-11-H-2[a]	2.1	0.12	−0.5	11.8	8.0	2.3	−24.39	0.02	2.05	0.63	43.51	
IHSC-11-H-3[a]	−5.4	−0.33	−1.3	2.1	8.7	−0.8	−1.55	0.01	1.41	0.51	38.01	
IHSC-11-P-1[a]	20.4	1.22	−0.3	2.3	9.4	0.3	−8.35	0.02	2.27	0.64	45.13	
IHSC-11-P-2[a]	−39.8	−2.39	−0.7	2.4	6.3	−0.1	−3.45	0.01	1.39	0.57	38.14	
IHSC-11-P-3	7.1	0.43	15.9	104.2	59.7	40.2	6.53	1.16	5.37	0.74	61.01	
IHSC-11 (H + P)	**9.7**	**0.6**	**17.6**	**54.0**	**41.3**	**30.2**	**3.4**	**1.04**	**3.8**	**0.7**	**53.0**	**3.67**
IHP-12-1[a]	−0.7	−0.04	1.2	13.4	81.8	4.7	11.63	−0.01	0.70	0.51	30.34	
IHP-12-2	12.2	0.73	2.8	16.1	95.2	7.0	5.81	0.26	0.84	0.54	32.32	
IHP-12-3	5.9	0.35	3.2	16.0	90.7	7.4	4.97	0.15	1.34	0.60	37.99	
IHP-12-4	4.2	0.25	5.2	24.6	97.7	11.4	4.70	0.16	1.20	0.59	37.02	
IHP-12-5	9.4	0.56	5.2	23.1	115.9	11.1	4.41	0.37	1.60	0.62	40.45	
IHP-12-6	0.7	0.04	1.6	8.6	51.6	3.8	5.48	0.01	1.59	0.62	40.55	
IHP-12	**6.5**	**0.4**	**3.6**	**17.7**	**90.2**	**8.1**	**5.1**	**0.19**	**1.3**	**0.6**	**37.7**	**4.48**
IHG-13-1	14.6	0.87	3.0	21.2	119.3	8.5	7.11	0.42	1.44	0.59	37.23	
IHG-13-2	20.7	1.24	1.8	8.6	52.7	4.1	4.74	0.39	16.31	0.81	88.29	
IHG-13-3	27.9	1.67	1.8	8.9	64.9	4.2	5.01	0.52	8.28	0.78	72.34	
IHG-13-4[a]	41.3	2.48	3.8	22.1	106.2	9.5	5.76	1.64	5.42	0.74	62.09	
IHG-13	**21.1**	**1.3**	**2.2**	**12.9**	**78.9**	**5.6**	**5.6**	**0.44**	**8.7**	**0.7**	**66.0**	**6.69**

Note. Each aliquot is listed with corresponding single-grain cooling ages. When multiple aliquots are dated, then the mean sample ages listed in bold font are reported with the standard error of the mean. ESR: equivalent spherical redius (microns).
[a]Aliquot not reported in the text and not used in mean sample ages due to analytical inconsistency from measurements (e.g., no measurable He; grains other than apatite measured; inclusions)

supporting information S2). The TT and MT are closely spaced thrusts in the middle of the Sub-Himalayan belt (Figures 2–4). A sample from the Lower Murree Formation in the MT hanging wall (IHM-16) has a mean age of 1.9 ± 0.6 Ma, whereas the Upper Murree Formation sampled between the MT and TT (IHM-16) yields a mean age of 10.2 ± 3.7 Ma (Figure 4, Table 3, and supporting information S2).

All mean sample AHe ages are younger than the stratigraphically constrained depositional age of the same sample (Figure 5a), indicating that AHe ages are reset. Scatter on limited mean sample ages and within single-grain age population of individual samples (Table 3) may reflect partially reset cooling ages due to a combination of different geologic conditions. Those conditions potentially include shallower stratigraphic burial and cooler paleotemperatures for the uppermost units (Middle Siwalik and Upper Siwalik Formations; Table 1), slower localized fault-related uplift, long residence in the AHePRZ for samples in the footwall of thrusts, and variations in closure temperature due to differences in eU concentration or grain size. We further constrain the thermal history of each sample by modeling individual single-grain data in section 6.

Plots of AHe cooling ages versus distance across the Sub-Himalayan structures indicate that cooling history varies as a function of structural position (Figure 6). For the SMA, young cooling is localized at the fold axis. Samples from the northeastern limb of the fold are older (partially reset at shallower burial depths and/or slow cooling). AHe ages from the core of the SMA range from 1.0 to 4.4 Ma (Figure 4). To the north, sample ages differ between hanging wall and footwall of the Sub-Himalayan faults. Both stratigraphically deeper (Murree) and shallower (Siwalik) footwall samples yield older AHe ages than hanging wall samples. Hanging wall samples of the RF/MKT and MT range from 1.9 to 3.0 Ma. Footwall samples are generally older, ranging from 5.6 to 10.2 Ma for the MKT, RF, and MT. This pattern is interpreted to result from differential exhumation across faults during shortening.

4.1.2. Hinterland Samples

Mean AHe ages from four hinterland samples range from 5.1 to 21.1 Ma (Figure 4, Table 3, and supporting information S2). Cooling ages are younger than the precollisional protolith ages, indicating the samples represent exhumation ages. These hinterland cooling ages (>5 Ma) are older than most of those from the foreland (<5 Ma). Sample IHR-10, located in the hanging wall of the MBT, south of the MCT, has a mean age of 5.1 ± 2.1 Ma. Two samples, IHSC-11 and IHP-12, north of the MCT in its hanging wall, have mean ages, of 9.7 ± 3.7 Ma and 6.5 ± 4.5 Ma, respectively (Figure 4, Table 3, and supporting information S2). Hinterland

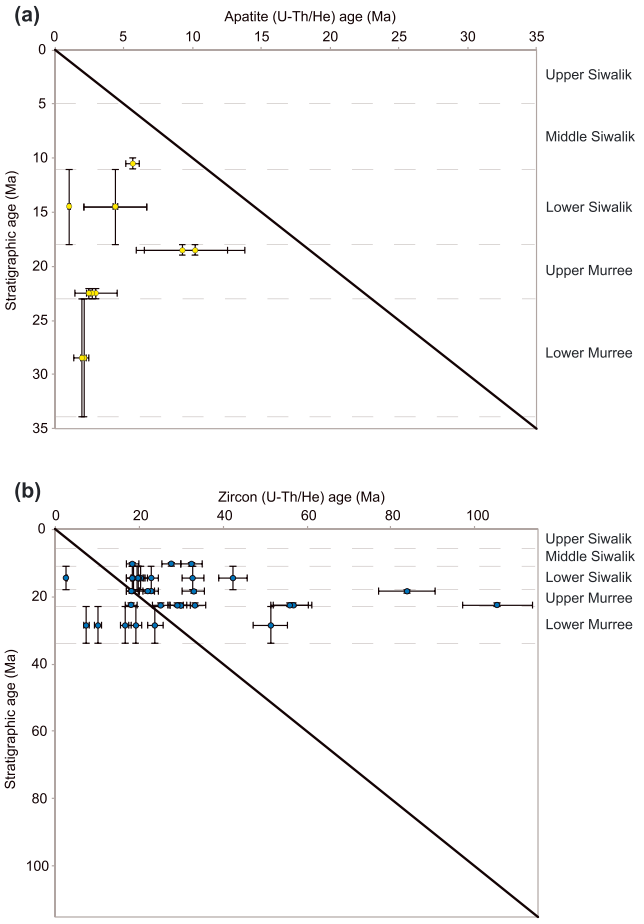

Figure 5. Cooling ages versus stratigraphic age of detrital foreland samples. Estimates of foreland unit stratigraphic ages are provided by data compilations for the northwest Himalaya and Pakistan in Burbank et al. (1996), Kumaravel et al. (2005), and Shah (2009). (a) AHe mean sample age data. The plot shows that most detrital AHe cooling ages, regardless of stratigraphic level, are younger than stratigraphic age, and thus are reset. (b) ZHe single-grain age data. The plot shows that with the exception of seven grains, most grains are older than or the same age as the sampled unit.

cooling ages between 10 and 5 Ma are generally consistent with expected upper crustal exhumation related to motion on the MBT (Brozovic & Burbank, 2000; Meigs et al., 1995; Sangode & Kumar, 2003). Further north of the MCT, a 21.1 ± 6.7 Ma age (IHG-13) suggests that the thrust sheet retains in parts an older exhumation history compatible with published constraints on MCT motion at ~20 Ma (DiPietro & Pogue, 2004; Hodges, 2000).

4.1.3. ZHe Data

ZHe ages were measured from the same samples as the AHe samples (Figure 4). All of the zircon cooling ages are older than the AHe ages from the same sample. In the foreland, ZHe data are reported in the text as single grain ages, since ZHe ages are generally older than the host unit's depositional age and not fully reset (Figure 5b). In the hinterland, ZHe data are reported as mean sample ages, as ZHe ages are uniformly younger than those of protoliths of the Lesser and High Himalaya rocks from which they were sampled. Table 4 provides a complete report of all mean sample and single-grain ZHe ages.

4.1.4. ZHe Foreland Samples

Foreland ZHe single-grain ages range from 2.7 to 105.4 Ma (Figure 4, Table 4, and supporting information S2). Most of these single grains are older than the stratigraphically constrained depositional ages (Figure 5b). We interpret these ages to represent older source-terrane cooling from which they were eroded prior to deposition, indicating ZHe ages have not been fully thermally reset during burial, in agreement with stratigraphic burial and paleotemperature estimates (Table 1). Notable exceptions include the stratigraphically deepest sample (10.3 and 7.5 Ma; zIHM-8-1 and zIHM-8-3) from the Lower Murree Formation, and from the Lower Siwalik Formation (2.7 Ma; zIHS-5-2) along the axis of the SMA (Figure 4, Table 4, and supporting information S2), Both samples include a number of ZHe single grain cooling ages that are significantly younger than the depositional age.

A large number of foreland single grain ZHe ages cluster within the age range of the hinterland bedrock ZHe samples and published ages for the MCT activity (foreland: 23–16 Ma; hinterland: 21–14 Ma; Figure 7). These data suggest that the sediments of the Siwalik and Murree Formations in the foreland are sourced from rocks exhumed and eroded along the MCT in the hinterland. Stratigraphic ages of the sampled units are not sufficiently well constrained to allow precise determination of the lag time between exhumation and deposition.

4.1.5. ZHe Hinterland Samples

Hinterland ZHe mean sample ages range from 13.3 to 22.5 Ma (Figure 4, Table 4, and supporting information S1). Three samples from the hanging wall of the MCT have ages of 13.3 ± 5.6 Ma (zIHSC-11), 18.1 ± 1.45 Ma (zIHP-12), and 22.5 ± 3.9 Ma (zIHG-13; Figure 4, Table 4, and supporting information S2). A fourth sample from the hanging wall of the MBT yields an age of 14.8 ± 7.5 Ma (zIHR-10). Given published constraints on the timing of thrust activity on the MBT and MCT, we interpret this cluster of 22–13 Ma ZHe ages (Figure 7) to reflect hinterland exhumation associated with shortening on the MCT and/or MBT (Burbank et al., 1996; Catlos et al., 2002; Kumar et al., 2003; Meigs et al., 1995; Metcalfe, 1993; Sangode & Kumar, 2003; Walker et al., 1999).

4.2. AFT Cooling Age Comparison

Published AFT and ZFT age data constrain hinterland exhumation from the KW northward to the ZSZ (Figure 4; Kumar et al., 1995). AFT cooling ages are younger (<3 Ma) within the KW duplex than in the thrust sheets above the MCT (Figures 4 and 6; Kumar et al., 1995). South of the KW, AFT ages are similar to our 4.5–7.2 Ma AHe ages from the Pir Panjal Range (Figures 4 and 6). North of the KW, AFT ages generally

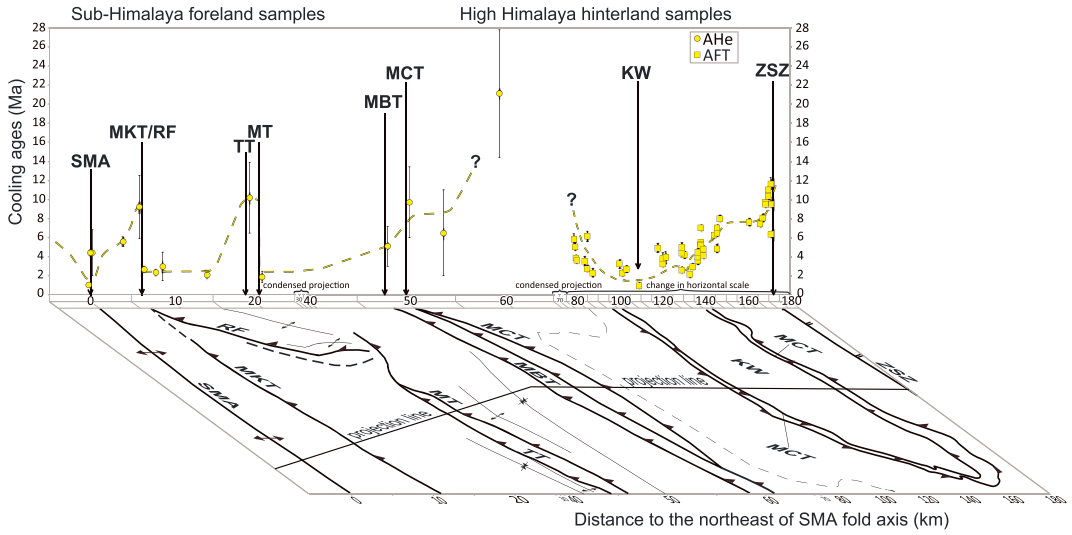

Figure 6. AHe and AFT cooling ages plotted against distance northeast of SMA along a NE-SW direction perpendicular to projection line. The solid circles and squares represent AHe and AFT ages, respectively, with associated uncertainties. See Figure 4 for sample location. Note that projection line is similar to cross section line B-B′-B″ and depicted with varying horizontal scales for illustrative purposes. Samples projected along strike of transects have been included. Full name abbreviations listed in Figure 2.

increase from south to north and define a pattern of progressively older cooling toward the ZSZ (Figures 4 and 6). An exception is the samples from a granitoid dome north of the KW that yielded AFT ages that are both older and younger than ~3 Ma (Kumar et al., 1995).

In comparison, AHe ages across the Sub-Himalayan structures are characteristically $<$4 Ma, which indicates that thrust-related exhumation of the foreland was synchronous with cooling recorded by AFT ages from the KW. Contemporaneous cooling and exhumation of structurally deep samples from the KW and the shallow imbricate thrust sheets of the Sub-Himalaya imply linkage between duplex growth in the hinterland and structural disruption of the foreland. In contrast, AHe cooling ages $>$3 Ma occur in the MBT/MCT thrust sheets structurally above the KW (Figures 4 and 6).

5. Thermal Model Results

We utilize thermal model results from QTQt on single-grain ages to constrain best fit t-T histories for each sample as a 2-sigma envelope. In using this approach, the modeling results are presented as a t-T area rather than a single path (Figure 8 and supporting information S1). For sedimentary samples (foreland) characterized by a combination of partially reset to fully reset AHe and ZHe ages, we increase accuracy and resolution of thermal history of each sample by overlapping model results from multiple individual single grain ages. Since each single-grain model swath represents the envelope through which any acceptable thermal history for an individual grain passes, we then interpret the overlapping area of model iterations of all single grains as the best fit thermal history for that sample (Sousa et al., 2017; Figure 8). For the metamorphic or igneous bedrock samples (hinterland) characterized with fully reset AHe and ZHe ages younger than the protolith ages, thermal models were run on single-grain aggregate models. A compilation of all thermal model results is included in supporting information S1.

AHe foreland sample thermal models are shown for the entire postdepositional history (Figure 8 and supporting information S1). Given AHe foreland samples are mostly fully reset (Figure 5a), the thermal models do not focus on the predepositional thermal history. Limited reset single-grain ZHe ages were also modeled, but these did not increase precision in the best fit thermal models when considered with the AHe data from the same samples (zIHS-5 and zIHM-8; Table 4 and supporting information S1). For the SMA at the deformation front (SMA; Figures 4 and 6), AHe single-grain t-T paths show that significant cooling was underway by 4 Ma. The depositional age of the sampled unit, the Lower Siwalik Formation (~18–11 Ma) in the case of the

Table 4
Kashmir Himalaya Zircon (U-Th)/He Data for Both Single-Grain and Mean Sample Ages

Sample num.	Age (Ma)	± (Ma)	U (ppm)	Th (ppm)	147Sm (ppm)	e (U)	Th/U	He (nmol/g)	Mass (ug)	Ft	ESR	Standard error of mean
Suruin-Mastgarh anticline (SMA)												
zIHS-1-1	18.4	1.47	531.1	65.3	1.4	546.1	0.12	41.4	5.61	0.76	48.00	
zIHS-1-2	42.4	3.39	457.9	100.1	0.5	480.9	0.22	84.1	5.36	0.76	48.75	
zIHS-1-3	32.8	2.63	366.6	64.4	0.5	381.4	0.18	52.2	5.52	0.77	50.20	
zIHS-1	31.2	2.5	451.9	76.6	0.8	469.5	0.2	59.2	5.5	0.8	49.0	12.05
zIHS-5-1	19.6	1.57	498.5	100.9	0.8	521.7	0.20	41.7	5.21	0.75	46.83	
zIHS-5-2	2.7	0.22	1936.1	274.8	2.2	1999.4	0.14	21.6	3.60	0.74	43.21	
zIHS-5-3	22.8	1.83	642.6	135.8	3.3	673.9	0.21	61.1	3.58	0.74	43.14	
zIHS-5	15.0	1.2	1025.7	170.5	2.1	1065.0	0.2	41.5	4.1	0.7	44.4	10.80
zIHS-6-1	19.8	1.59	555.6	76.5	0.9	573.2	0.14	47.4	8.32	0.77	50.60	
zIHS-6-2	20.4	1.63	673.9	88.6	1.6	694.3	0.13	56.6	4.06	0.74	43.92	
zIHS-6-3	18.6	1.49	593.5	154.0	1.0	629.0	0.26	46.7	4.13	0.74	44.07	
zIHS-6	19.6	1.6	607.7	106.4	1.2	632.2	0.2	50.3	5.5	0.8	46.2	0.92
Mandili-Kishanpur thrust (MKT)												
zIHM-3-1	105.4	8.43	101.4	69.9	2.8	117.5	0.69	46.5	2.41	0.69	37.25	-
zIHM-4-1	33.3	2.67	504.2	45.4	0.6	514.6	0.09	66.7	2.91	0.72	40.04	
zIHM-4-2	56.6	4.53	102.4	51.7	1.0	114.3	0.50	26.1	5.01	0.74	45.49	
zIHM-4-3	29.8	2.39	442.6	431.7	1.2	542.0	0.98	65.5	5.94	0.75	46.91	
zIHM-4	39.9	3.2	349.7	176.3	1.0	390.3	0.5	52.7	4.6	0.7	44.1	14.57
zIHM-14-1	25.2	2.01	689.0	327.2	1.3	764.3	0.47	79.8	6.08	0.77	50.36	
zIHM-14-2	29.1	2.33	135.5	95.6	1.2	157.5	0.71	18.4	5.16	0.74	45.55	
zIHM-14-3	55.8	4.47	163.2	102.9	1.5	186.9	0.63	42.2	4.56	0.74	45.93	
zIHM-14-4	18.1	1.45	1474.2	79.3	0.7	1492.4	0.05	109.6	4.85	0.75	45.32	
zIHM-14	32.1	2.6	615.5	151.2	1.2	650.3	0.5	62.5	5.2	0.8	46.8	16.49
Riasi fault system (RF)												
zIHS-7-1	27.7	2.22	291.2	83.7	0.7	310.5	0.29	38.8	16.60	0.83	71.24	
zIHS-7-2	32.6	2.61	230.2	72.7	1.7	247.0	0.32	37.0	21.03	0.85	80.46	
zIHS-7-3	18.5	1.48	369.4	73.4	0.8	386.3	0.20	32.2	16.53	0.83	71.51	
zIHS-7	26.3	2.1	297.0	76.6	1.1	314.6	0.3	36.0	18.1	0.8	74.4	7.15
zIHM-8-1	10.3	0.82	697.4	91.8	0.8	718.6	0.13	29.1	3.59	0.73	42.43	
zIHM-8-2	16.8	1.35	117.2	36.7	0.5	125.7	0.31	9.0	15.56	0.79	55.98	
zIHM-8-3	7.5	0.60	255.9	127.3	1.7	285.2	0.50	8.7	4.92	0.75	46.35	
zIHM-8	11.5	0.9	356.9	85.3	1.0	376.5	0.3	15.6	8.0	0.8	48.3	4.77
zIHM-9-1	18.5	1.48	613.4	101.8	3.1	636.9	0.17	49.9	9.30	0.79	54.35	
zIHM-9-2	21.9	1.75	173.5	50.7	0.8	185.2	0.29	16.4	4.16	0.75	45.32	
zIHM-9-3	18.5	1.48	484.0	107.0	0.9	508.7	0.22	39.3	6.01	0.77	50.45	
zIHM-9	19.6	1.6	423.6	86.5	1.6	443.6	0.2	35.2	6.5	0.8	50.0	1.98
Tanhal thrust (TT) and Mundun thrust (MT)												
zIHM-15-1	22.8	1.82	208.9	102.0	2.1	232.4	0.49	21.5	4.64	0.75	46.89	
zIHM-15-2	32.9	2.63	174.7	125.3	0.8	203.6	0.72	27.0	4.66	0.74	45.96	
zIHM-15-3	83.8	6.70	192.0	120.6	0.8	219.8	0.63	71.5	3.05	0.71	40.56	
zIHM-15	46.5	3.7	191.9	116.0	1.3	218.6	0.6	40.0	4.1	0.7	44.5	32.68
zIHM-16-1	51.4	4.11	150.8	123.9	1.9	179.3	0.82	36.6	3.88	0.73	43.92	
zIHM-16-2	23.9	1.91	340.8	46.6	1.2	351.5	0.14	35.4	8.04	0.78	52.61	
zIHM-16-3	19.1	1.53	88.8	42.1	0.7	98.5	0.47	7.7	4.83	0.75	47.27	
zIHM-16	31.4	2.5	193.5	70.9	1.3	209.8	0.5	26.6	5.6	0.8	47.9	17.41
MBT/MCT (Pir Panjal Range)												
zIHR-10-1	20.9	1.67	653.5	62.5	0.6	667.9	0.10	61.4	11.53	0.82	62.84	
zIHR-10-2	17.1	1.37	433.6	125.0	0.5	462.4	0.29	33.9	7.34	0.79	56.86	
zIHR-10-3	6.4	0.51	38.2	36.6	2.0	46.7	0.96	1.2	3.10	0.72	41.91	
zIHR-10	14.8	1.2	375.1	74.7	1.0	392.3	0.4	32.1	7.3	0.8	53.9	7.51
zIHSC-11-P-1	19.1	1.53	230.3	62.7	1.2	244.7	0.27	20.2	10.39	0.80	59.08	
zIHSC-11-P-2	12.9	1.03	1047.6	557.6	8.0	1176.0	0.53	60.0	3.90	0.73	43.10	
zIHSC-11-P-3	7.9	0.63	925.9	132.3	1.5	956.4	0.14	30.7	5.03	0.76	46.99	
zIHSC-11 (P)	13.3	1.1	734.6	250.9	3.6	792.4	0.3	37.0	6.4	0.8	49.7	5.62
zIHP-12-1	18.1	1.45	236.0	60.3	0.9	249.9	0.26	18.6	4.83	0.76	47.90	–
zIHG-13-1	18.1	1.45	93.9	79.5	6.5	112.2	0.85	8.8	11.45	0.80	59.90	
zIHG-13-2	24.1	1.92	95.7	64.5	1.7	110.5	0.67	11.3	9.06	0.79	56.38	

Table 4 *(continued)*

Sample num.	Age (Ma)	± (Ma)	U (ppm)	Th (ppm)	147Sm (ppm)	e (U)	Th/U	He (nmol/g)	Mass (ug)	Ft	ESR	Standard error of mean
zIHG-13-3	25.4	2.03	149.3	109.5	4.3	174.5	0.73	18.3	6.03	0.76	49.94	
zIHG-13	22.5	1.8	112.9	84.5	4.1	132.4	0.8	12.8	8.8	0.8	55.4	3.89

Note. Each aliquot is listed with corresponding single-grain cooling ages. When multiple aliquots are dated, then the mean sample ages are listed in bold font, reported with standard error of the mean. ESR: Equivalent spherical radius (microns).

SMA, constrains the maximum permissible onset of cooling. Cooling must postdate the younger bounding age of the sampled formation (Figure 8a and supporting information S1; Burbank et al., 1996). For the hanging wall samples exposed in Sub-Himalayan faults (RF, MKT, and TT; Figures 4 and 6), AHe single-grain t-T paths show that significant cooling was ongoing between 2 and 4 Ma (Figure 8b and supporting information S1).

Hinterland sample initial thermal conditions during deposition of the protoliths are not shown in the models because their depth and prior metamorphic history are unconstrained prior to the youngest cooling events (supporting information S1). Thermal models were run on limited set of samples combining AHe and ZHe ages. No demonstrable change in cooling in the last ~5 Myr are revealed by the data in the Pir Panjal Range (Figure 4 and supporting information S1). Time-temperature paths on a sample location within the MCT thrust sheet indicate significant cooling between approximately 18 and 13 Ma from combined ZHe data and AHe data (IHS-11; supporting information S1), likely associated with thrust activity of the MCT.

5.1. Exhumation Rates

The thermal history envelope resultant from overlapping single-grain and mean age models allows for direct measurement of cooling rates over a time confined by the models. Using our assumed modern surface temperature of 20 °C for the Sub-Himalayan belt, we calculate minimum and maximum values for each foreland sample from 1 Ma to present and 4 Ma to present. Additionally, these cooling rates can be converted to exhumation rates by assuming a geothermal gradient of ~ 20 °C/km in the Sub-Himalaya (18–24 °C/km from Agarwal et al., 1994; van der Beek et al., 2006). Table 5 lists calculated exhumation rates both from the last 1 Myr (maximum) and 4 Myr (minimum) for the youngest mean sample AHe ages of each the major structures.

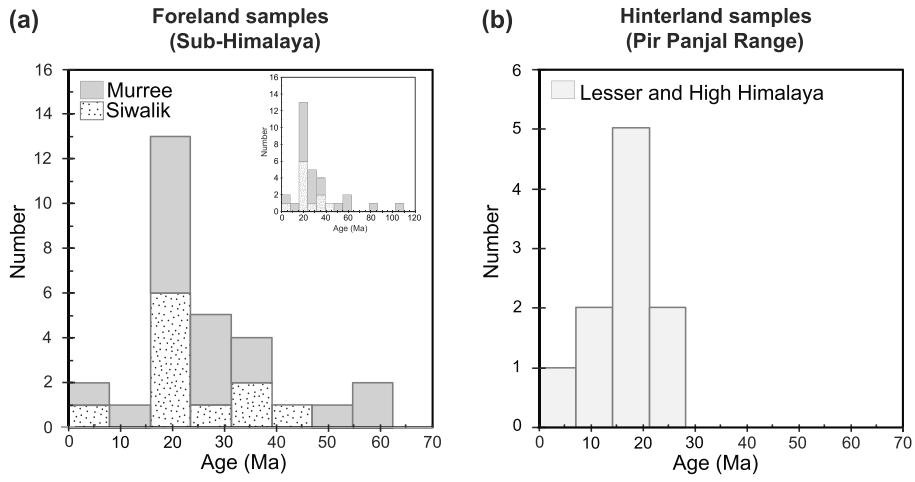

Figure 7. Zircon (U-Th)/He single-grain age distributions of (a) foreland detrital samples in the Sub-Himalayan belt (Murree and Siwalik Formations) and (b) hinterland bedrock samples across the MBT and MCT thrust sheets in the Pir Panjal Range. See Figure 4 for location. Insert plot in (a) depicts single grain ages older than 70 Ma. The plots reveal that a large number of grains in the foreland domain cluster in the 16–23 Ma age range, similar to a cluster of grains in the hinterland that span the same time interval.

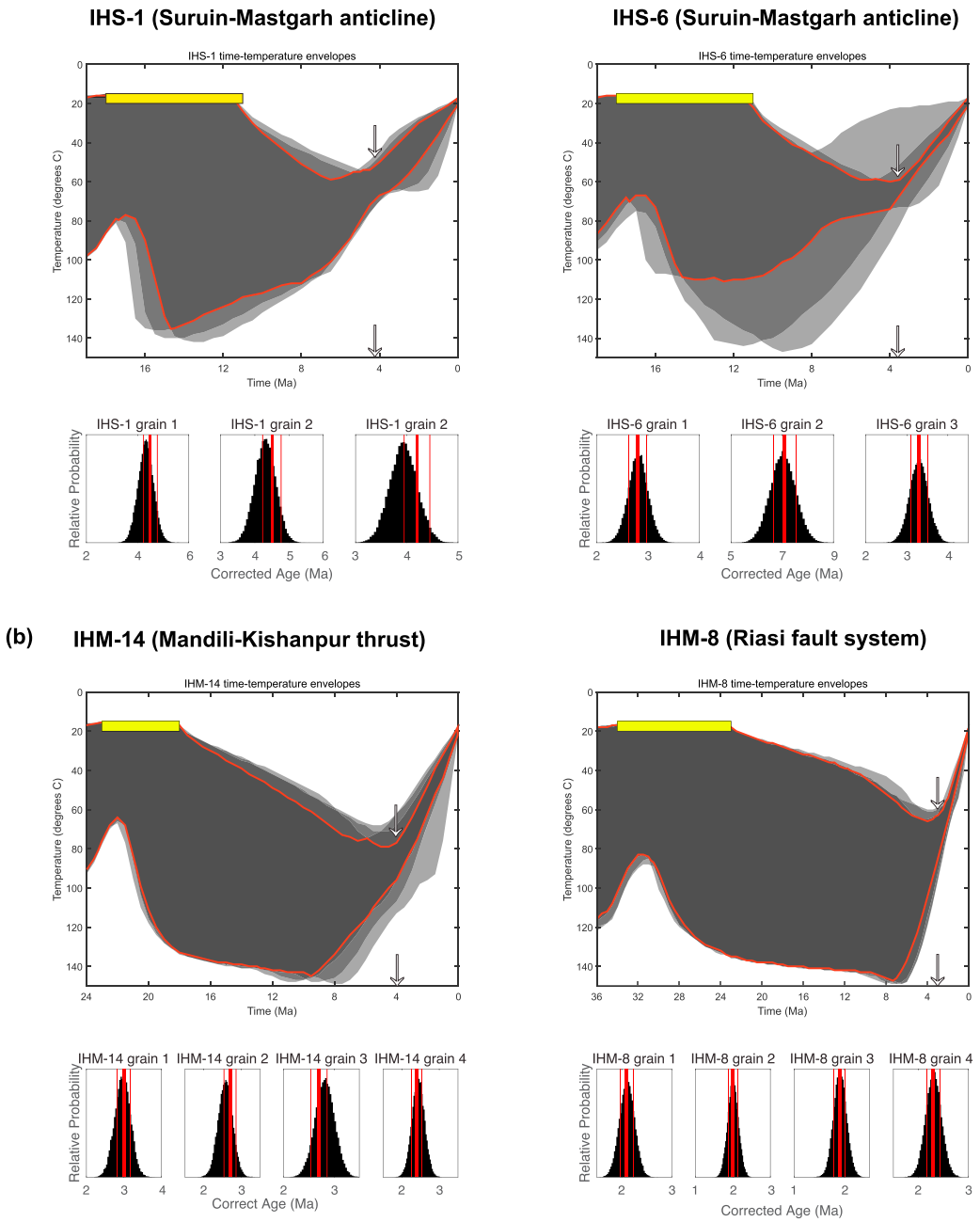

Figure 8. Thermal history model results using QTQt from a subset of foreland samples (a) in the core of the Suruin-Mastgarh anticline (SMA; IHS-5 and IHS-6) at the deformation front, (b) in the hanging wall of Sub-Himalayan faults on the Mandili-Kishanpur thrust (MKT; IHM-14) and on the Riasi fault system (RF; IHM-8). See Figure 4 for location and Table 3 for respective thermochronologic AHe age data. Top: Envelopes of acceptable time-temperature paths for each individual grain age data are shown in grey, with overlapping best fit regions shown in black and highlighted in red. Model input parameters are listed in Table 2, which include depositional age, surface temperature, time-temperature bounding box, and assumed geothermal gradients. Bottom: Histograms and relative probability plots of predicted model ages (black histogram) compared to the observed age (the thick red bar is observed age; the thin red bar are uncertainties) for each single grain age data. The model ages agree with the observed single grain ages see supporting information S1 for compilation of thermal model results for the other foreland and hinterland samples.

Using this technique, exhumation rates over the last 1 Myr from the southernmost three foreland samples taken from the SMA range from 0.5 to 2.4 mm/year (Table 5; Figures 4 and 9). Net long-wavelength incision from folded Pleistocene terraces across the SMA suggests rock uplift rates of ~2 mm/year (Gavillot, 2014), which is in agreement with the rate determined from the thermal models. Post–1 Ma exhumation rates

Table 5
Exhumation Rates for AHe and AFT Data in the Kashmir Himalaya

	Exhumation rate estimates (mm/year)	
Sample/location	1–0 Ma	4–0 Ma
AHe data		
IHS-1	0.5	0.48
IHS-5	2.35	1.03
IHS-6	0.63	0.59
SMA (avg)	1.16 ± 1.03	0.7 ± 0.29
IHM-3	0.95	0.71
IHM-4	0.83	0.53
IHM-14	0.9	0.83
MKT (avg)	0.89 ± 0.06	0.69 ± 0.15
IHS-7 (RF footwall)	1.03	0.36
IHM-9 (RF footwall)	0.43	0.24
IHS-8 (RF hanging wall)	1	0.82
IHM-15 (MT footwall)	0.3	0.22
IHM-16 (MT hanging wall)	1.15	1.16
IHR-10 (MBT)	0.2	0.23
IHSC-11 (MCT)	0.14	0.09
AFT data		
Kishtwar Window (KW)	3.2–3.6[a]	
High Himalaya Range	0.33–0.35[b]	
Zanszkar Shear Zone (ZSZ)	0.02–0.18[b]	

[a]Equation-derived exhumation rates (Kumar et al., 1995). [b]Vertical transect-derived exhumation rates (Kumar et al., 1995).

from samples taken from other Sub-Himalayan thrusts north of the SMA range from 0.8–1 mm/year for the MKT to 1 mm/year for the RF and 1.2 mm/year for the MT (Table 5; Figures 4 and 9).

Post–4 Ma exhumation rates determined from the thermal models provide long timescale estimates consistent with the cluster of <4 Ma AHe ages from the SMA and Sub-Himalayan faults (Figures 4, 6, 8, and 9 and supporting information S1). For the SMA these rates range from 0.5–1 mm/year, while those from Sub-Himalayan faults to the north range from 0.5–0.8 mm/year for the MKT, to 0.8 mm/year for the RF, and 1.2 mm/year for the MT.

The thermal models are also used to calculate exhumation rates for the hinterland samples north of the MBT using mean AHe age data (supporting information S1) and on the same timescale (1–0 Ma and 4 –0 Ma; Table 5) for comparison with the Sub-Himalayan structures. Together with published exhumation rates from the KW to the ZSZ, these rates reveal strong spatial variability from south to north across the Kashmir Himalaya (Figure 9). Using an average surface temperature of 10 °C, cooling rates are converted to exhumation rates by assuming a geothermal gradient of 30–45 °C (Deeken et al., 2011; Kumar et al., 1995). In the Pir Panjal Range, cooling ages and thermal modeling data from the MBT and MCT thrust sheets imply lower exhumation rates (0.1–0.2 mm/year) than in the Sub-Himalaya (Table 5). At the KW (Figure 9), AFT data suggest that exhumation rates are high within the structure, ranging from 3.6 mm/year from Kumar et al. (1995) to 3.2 mm/year based on geothermal gradients of 30 and 45 °C, respectively. Such estimates of exhumation rates are calculated using 1-D kinematic equation $E_r = ([T_c - T_s]/A)/(dT/dz)$, as defined similarly in Dodson (1973) and Blythe et al. (2007), in which T_c is the known closure temperature, T_s the average surface temperature, A is the sample age since cooling, and dT/dz is the assumed geothermal gradient. Further north in the upper plate of the KW (Figure 9), exhumation rates decrease to the northeast from 0.33 to 0.35 mm/year derived from available vertical transects in the High Himalaya Range and 0.02 to 0.18 mm/year across the ZSZ derived from E_r equation calculations (Kumar et al., 1995). Comparison of hinterland exhumation rates to the southeast of the Kashmir Himalaya also reveals along-strike spatial variability (Figure 9). AFT data and vertical transects from Deeken et al. (2011) indicate that apparent exhumation rates are 2.8 mm/year for the MBT/MCT thrust sheets in the Dhauladhar Range at the topographic front of the High Himalaya but are lower (<1 mm/year) further north across the High Himalaya (Figure 9).

6. Discussion

6.1. Space-Time Pattern of Thrusting Across the Kashmir Himalaya

AHe cooling ages from sedimentary samples exposed in folds and faults in the Sub-Himalayan foreland reveal a pattern of distributed deformation established by 4 Ma (Figures 4, 6, 8). Samples from along the core and flanks of the SMA fold at the deformation front (Figures 1,2, 3) yield mean ages between 1 and 4.4 Ma (Figure 4). Single-grain AHe data indicate dispersal of ages ranging between 0.9 and 7.1 Ma (Table 3). Thermal modeling of these grains indicate that cooling was underway 4 Ma (Figure 8a and supporting information S1). We interpret this cooling as a record of thrust-related folding and exhumation at the deformation front. These data do not exclude the possibility that thrust-related exhumation initiated before 4 Ma, as indicated by the thermal models (Figure 8; supporting information S1), depositional age constraints of the sampled units (Burbank et al., 1996), and structural restorations (between 4 and 10 Ma; Figure 10). An onset of thrust-related folding ~4 Ma at the deformation front is significantly earlier than the ~1.7 Ma initiation age of thrust-related uplift inferred from a decrease in Upper Siwalik sedimentation accumulation rate (Ranga Rao et al., 1988) but is more similar to the ~5.5 Ma age of onset of the Salt Range thrust at the leading edge of the Pakistan Himalaya to the west (Figure 1; Burbank & Beck, 1989). To the north within the Sub-Himalaya, samples from unroofed foreland strata exposed in the hanging wall of the Riasi, Mandili-Kishanpur, and Mundun

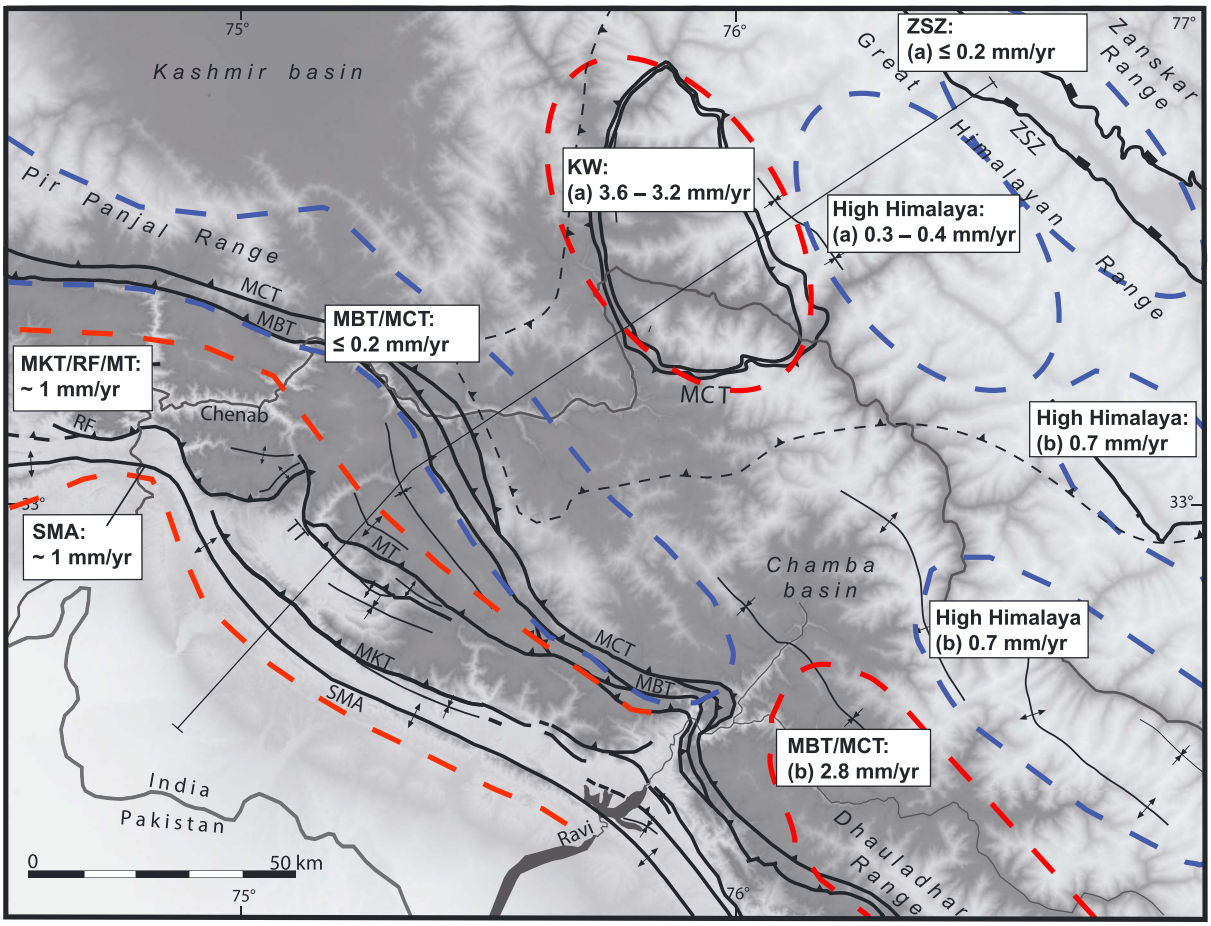

Figure 9. Regional distribution of calculated AHe and AFT exhumation rates derived from average estimates using QTQt thermal model (Table 5), published exhumation equations (after Dodson, 1973), and vertical relief transects. See text for explanation. Note the locations of high exhumation rates shown in red dashes both for the Sub-Himalayan structures (Suruin-Mastgarh anticline [SMA], Mandili-Kishanpur thrust [MKT], Riasi fault system [RF], and Mundun thrust [MT]), and a structural window (KW) in the hinterland. (a) Exhumation rates derived from AFT age data from Kumar et al. (1995). (b) Exhumation rates to southeast of our study area from Deeken et al. (2011). Full name abbreviations listed in Figure 2.

fault systems (RF, MKT, and MT, respectively; Figure 4) yield a narrow age range between 1.9 and 3.0 Ma (Figures 4 and 6). Single-grain AHe data show minimal dispersal (1.3 to 4.1 Ma; Table 3), and thermal models constrain cooling to be underway between 2 and 4 Ma, with high exhumation rates of ≥1 mm/year for the Sub-Himalayan structures (Figures 8 and 9; supporting information S1). Our timing constraints represent a minimum for the onset of thrust-related exhumation across the Sub-Himalayan faults (RF, MKT, and MT). Restoration, structural positions, and depositional constraints of the timing of these thrusts suggest that thrusting could have initiated anytime between 4 and 10 Ma (Figure 8b, 10), as indicated by the thermal models (Figure 8b and supporting information S1). Samples from the footwall of the RF and MT have mean AHe ages of 9.2 and 10.2 Ma, respectively, which are markedly older than other samples in the Sub-Himalaya, and come from the Upper Murree Formation (approximately 23–18 Ma stratigraphic age; Figure 5; Burbank et al., 1996). Interpreted as the result of thrust-related exhumation, those cooling ages would indicate initial disruption of the foreland close in time to formation of the MBT at approximately 11 Ma (Meigs et al., 1995). This interpretation seems unlikely given that the kinematic restoration and structural positions of the RF and MT footwalls in the upper plate of other Sub-Himalayan thrust sheets require fault-related exhumation to have occurred between 4 and 10 Ma (Figure 10). A more reasonable interpretation is that these older ages were only partially reset by burial.

AHe and ZHe cooling also constrain thrust-related exhumation of the Pir Panjal Range, the hinterland front range to the north of the MBT, ranging between 5.1 and 22.5 Ma (Figure 4). A sample from the hanging wall of the MBT from a tributary of the Chenab River Valley has a 5.1 Ma AHe age (Figure 4). Three samples from

the MCT thrust sheet range in age from 6.5 to 21.1 Ma and have uncertainties ~30 and 70% of the age, respectively. ZHe ages from thrust sheet samples are 14.8 for the MBT and 13.3–22.5 Ma for the MCT. We conservatively interpret these ages to reflect minimum constraints for the exhumation related to motion on the MBT and MCT and passive translation of those thrust sheets along the MHT detachment. ZHe and AHe age data delineate an exhumation history that coincides with early motion on the MCT starting prior to 22 Ma (ZHe), including possible protodisplacement on the MBT. Low exhumation rates (0.1–0.2 mm/year) from the MBT and MCT thrust sheets imply continuing cooling and exhumation until 6.5 Ma (AHe) for the MCT and 5.1 Ma (AHe) on the MBT are likely associated with passive movement along the MHT (Figure 10). The age range of thrusting inferred from these data in the Kashmir Himalaya is consistent with other comparable age and kinematic constraints across individual hinterland thrusts elsewhere in the Himalaya (DiPietro & Pogue, 2004; Hodges, 2000; Yin, 2006, and references therein). Our age data and thermal models do not support the hypothesis that significant thrust-induced exhumation has occurred in the last few millions years on the MBT and MCT as suggested in previous interpretations (e.g., DiPietro & Pogue, 2004; Nakata, 1989; Stephenson et al., 2000; Wadia, 1934). Geomorphic data also reveal no evidence of motion on the MBT since at least 14–17 kyr (Vassallo et al., 2015; Vignon, 2011).

Further north, FT data across the KW indicate that cooling within the window beneath the MCT roof thrust is younger than in the overriding thrust sheets structurally above the window (Figures 3, 4, and 6; Kumar et al., 1995). Cooling ages between 1 and 3 Ma and exhumation rates of ~ 3 mm/year (Table 5) characterize rocks sampled along the Chenab River within the structural window. Rocks sampled above the MCT roof thrust to the south and north of the KW, including the High Himalaya Range, record generally older cooling ages (3.1–6 Ma and $>$6 Ma; Figures 4 and 6), where vertical transects imply lower exhumation rates ($<$0.4 and $<$0.2 mm/year; Table 5). ZFT ages are older than 6 Ma (Figure 4; Kumar et al., 1995). Thus, the cooling pattern across the hinterland demonstrates that younger ages and a higher exhumation rate characterize the core of the KW structural culmination, which contrasts from structurally bounding higher thrust sheets. A recent thermochronologic study on an hinterland duplex structure in Himachal Pradesh, further to the southeast, near the Rampur window, indicate similar high exhumation rates (2–3 mm/year) since the Pliocene time (Stübner et al., 2018).

We infer that duplex development due to horse emplacement above the MHT at depth (the basal décollement; Figure 10) controls the locus of exhumation associated with the KW (DiPietro & Pogue, 2004; Searle et al., 2007; Yin, 2006). Horse emplacement at depth produces localized regions of relatively high uplift rates (Boyer & Elliott, 1982; Gilluly, 1960; Molnar & Lyon-Caen, 1988; Oriel, 1950), a mechanism invoked to explain young cooling ages and fault-related exhumation across structural culminations in the Nepalese hinterland (Bollinger et al., 2006; Brewer & Burbank, 2006; Herman et al., 2010; Robert et al., 2009) and in the Sikkim Himalaya hinterland (Abrahami et al., 2016; Landry et al., 2016). Similarly, young cooling ages characterize the Rampur window, another hinterland structural window in the neighboring western Himalaya (Lal et al., 1999; Schlup et al., 2003; Thiede et al., 2004; Thiede et al., 2005; Thiede et al., 2009; Vannay et al., 2004).

Thrust belt growth via duplex formation requires that horse emplacement at depth in the hinterland must be balanced by shortening on structures updip along the basal décollement and/or by faults that branch from roof thrusts (Boyer, 1992; Boyer & Elliott, 1982). The observation that exhumation of folds and faults that deform the foreland was contemporaneous with exhumation of the KW (Figure 4) favors the interpretation that foreland shortening is tectonically linked with crustal growth of the hinterland structural culmination represented by the KW (Figure 10). Foreland folds and thrusts record exhumation after ~4 Ma synchronous with the 1–3 Ma cooling ages from the core of the KW. Had shortening been passed onto the MCT roof thrust above the window, cooling ages within the MCT thrust sheet between the KW and the MCT fault trace to the south, in the hinterland front range (Pir Panjal Range), would be of the same age or younger than those within the Kishtwar duplex. Cooling history of the KW and Sub-Himalayan structures affecting the foreland reflects an in-sequence structural development in which horse formation in a duplex folds the upper plate, provides a mechanism for exhumation into the lower plate, and passes that shortening toward the foreland periphery of the thrust belt (e.g., Boyer & Elliott, 1982; Burbank et al., 1992; Price, 1981). Estimated erosion rates (Figure 9; Table 5) reinforce the interpretation that spatially variable exhumation reflects a temporal linkage between deep structural processes in the hinterland and deformation of the thrust belt margin (Molnar & Lyon-Caen, 1988).

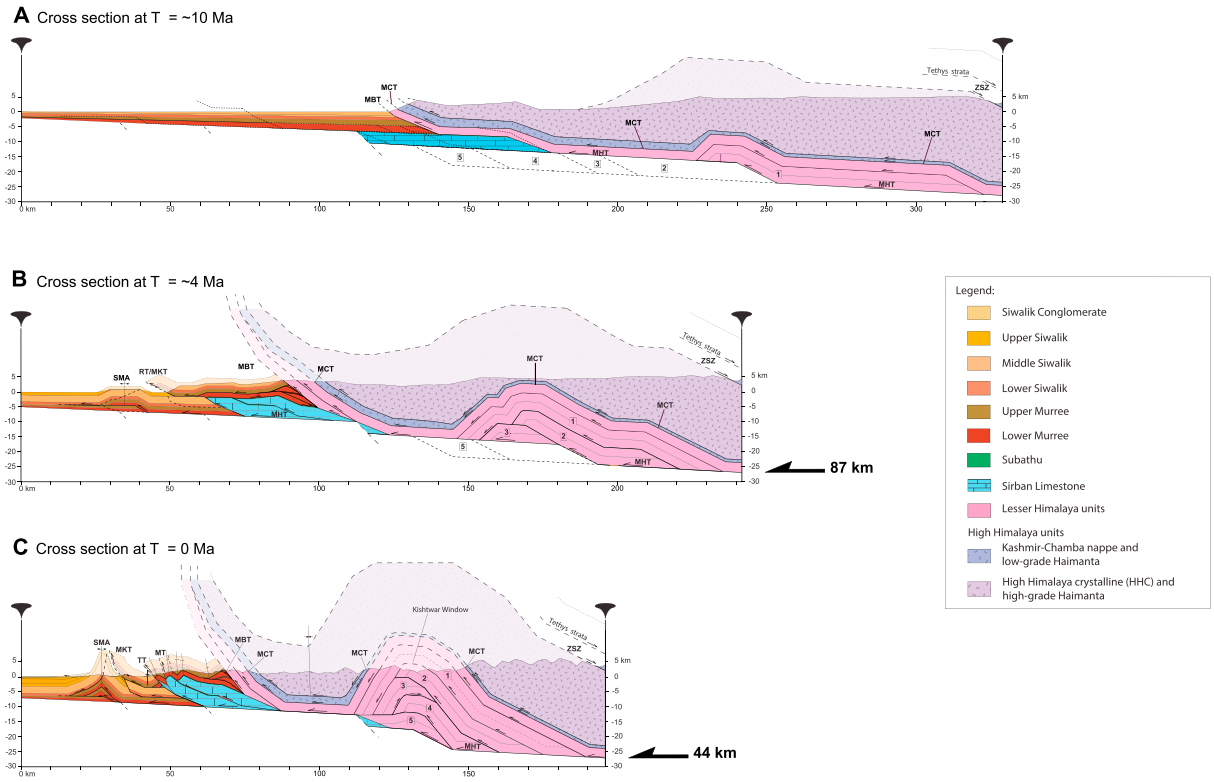

Figure 10. Sequential balanced restoration of cross section A-A″ from Figure 3 at (a) $T = 10$ Ma, (b) $T = 4$ Ma, and (c) $T = 0$ Ma (present). Stratigraphic age relations and geometric restorations of Sub-Himalayan and High Himalayan thrust sheets constrained by thermochronometric data from this study, and published data in Northwest Himalaya (Meigs et al., 1995; Powers et al., 1998, Thakur & Rawat, 1992; DiPietro & Pogue, 2004). Stratigraphic ages and fault name abbreviations given in Figure 2. As a note, Precambrian Sirban Limestone and Lesser Himalaya strata are age equivalent after Thakur and Rawat (1992), but a direct age relation is unknown between the two units.

The sequence of thrusting within the Sub-Himalaya is more complicated. Exhumation related to growth of the SMA at the deformation front was underway by 4 Ma and continued until after 1 Ma (Figures 4, 8a). The data suggest that accretion of the foreland due to propagation of the basal décollement southward to the position of the SMA was contemporaneous with or shortly followed cessation of displacement on the MBT after ~5 Ma (Gavillot et al., 2016; Kumar et al., 2003). Displacement on the MBT at ~5 Ma is consistent with cooling ages and kinematic data in the Nepalese Himalaya (DeCelles et al., 2001; DeCelles, Gehrels, Quade, & Ojha, 1998; Yin, 2006). A ~4 Ma initiation age for Sub-Himalayan shortening overlaps with growth of the Salt Range thrust in Pakistan (Burbank & Beck, 1989) but is ~2 Ma earlier than previous studies in the Kashmir foreland (Ranga Rao et al., 1988) and of structures in the Nepal foreland (Mugnier et al., 2004; van der Beek et al., 2006). Our data do not indicate whether thrusts between the SMA and MBT also initiated ~4 Ma, but they clearly demonstrate that structurally controlled exhumation was underway by 2–4 Ma (Figures 4, 6, 8b). Distributed deformation by imbricate thrusting and folding in the Sub-Himalayan foreland structures thus balances horse emplacement beneath the hinterland over the past ca. 4 Myr

6.2. Qualitative Comparison of Structural Evolution With Critical Wedge Model Predictions

Critical wedge theory provides a framework for interpreting orogenic evolution in the context of tectonic and erosional fluxes, spatial patterns of active deformation, changes in erosional efficiency, and other variables. Long-term translation occurs when an orogenic wedge attains a critical taper (Davis et al., 1983; DeCelles & Mitra, 1995; Meigs & Burbank, 1997). Critical taper is a geometrical state characterized by a surface slope and basal décollement angle that results in stress everywhere within the brittle wedge being close to failure (Dahlen & Suppe, 1988; Davis et al., 1983). Growth and change of an orogenic belt thus depends on the relative proportion of mass added relative to mass removed via erosion (Molnar & Lyon-Caen, 1988; Willett et al., 1993). Underplating and frontal accretion represent two key mechanisms by which mass is added to an

orogenic wedge (Boyer & Elliott, 1982; Gutscher et al., 1998; von Huene & Scholl, 1991). Underplating, the structural transfer of material from the lower, downgoing plate to the upper plate (e.g., via creation of a structural duplex), causes orogenic thickening (Boyer & Elliott, 1982; DeCelles & Coogan, 2006; Molnar & Lyon-Caen, 1988). Thrust propagation into undeformed sediment accretes material to the leading edge of a wedge (Davis & Hyndman, 1989; Gutscher et al., 1998; Hoth et al., 2006; Meigs & Burbank, 1997). Thrust front relocation into the undeformed foreland occurs when a wedge has a critical (or super critical) taper (Boyer, 1995; DeCelles & Mitra, 1995). Frontal accretion thus represents a short-lived widening and a subsequent shift to a subcritical state (Meigs & Burbank, 1997). Internal deformation by synchronous or out-of-sequence thrusting acts to rebuild taper (Boyer, 1992, 1995; Hoth et al., 2006, 2007; Morley, 1988; Vergés & Burbank, 1996; Vergés & Muñoz, 1990). Orogen narrowing by internal deformation behind the thrust front, by ongoing duplex development and/or thrust reactivation, occurs in response to instantaneous widening by accretion (Gutscher et al., 1996, 1998; Hoth et al., 2006, 2007). Narrowing and internal deformation are the expected responses to excess erosional mass removal relative to the tectonic mass influx as well (Davis et al., 1983; Whipple & Meade, 2004; Willett, 1999; Willett et al., 1993).

Our data indicate that internal deformation has been localized across the deformed Sub-Himalayan foreland and in the KW hinterland since at least ~4 Ma. In fact, deformation on the Kishtwar duplex has been likely ongoing since ~10 Ma (Figure 10), as is seen elsewhere in the Himalaya (Yin, 2006, and references therein). Prior to ~4 Ma, the thrust front was accommodated by proto thrusts of the MKT/RF (Figure 10). At ~4 Ma, the thrust front relocated further south on the SMA and accreted a portion of the Sub-Himalayan foreland to the wedge. The accretion event suggests that the wedge instantaneously widened at ~4 Ma. Subsequent deformation narrowed and built taper of the Kashmir wedge after 4 Ma. Deformation manifested by thrust-related exhumation was distributed between the Kishtwar duplex, at midcrustal depths and thrusting across the Sub-Himalaya faults in the upper-crust (Figure 10). This partitioning of shortening and sequence of events are the expected responses of a subcritical wedge to frontal accretion and concomitant decrease in wedge taper.

6.3. Climate Versus Tectonic Control on Exhumation

Low-temperature thermochronologic data from the hinterland provide one test of the hypothesis that climate, because of its linkage with erosional efficiency (Whipple & Meade, 2004, 2006; Whipple & Tucker, 1999), controls the pattern of deformation in the Himalaya. Most studies focus on the topographic break from low to high relief and mean elevation that focuses orographic precipitation (Bookhagen & Burbank, 2006; Bookhagen & Burbank, 2010; Hodges et al., 2001, 2004; Wobus et al., 2006). One body of literature argues that out-of-sequence thrusting driven by climate-enhanced erosion explains localized exhumation across the physiographic transition (e.g., Deeken et al., 2011; Grujic et al., 2006; Hodges et al., 2004; Huntington & Hodges, 2006; Jain et al., 2000; Thiede et al., 2004, 2005; Wobus et al., 2003; Wobus et al., 2005). Others maintain that overthrusting, duplex formation, and translation across a midcrustal ramp on the MHT explain the same pattern of young cooling ages (e.g., Bollinger et al., 2006; Brewer & Burbank, 2006; Herman et al., 2010; Robert et al., 2009; van der Beek et al., 2016; Whipp et al., 2007). We assess the relative degree of coupling or decoupling between climate and tectonic forcing on the exhumation pattern across the Kashmir Himalaya (1) by comparing thermochronometric with topographic and precipitation data across the structural transect in Figure 11 and (2) by comparing with neighboring structural, thermochronometric, and precipitation data across a Himalayan transect southeast of the Ravi River (Figure 1; Deeken et al., 2011).

Precipitation data from the Kashmir Himalaya (Bookhagen & Burbank, 2006), topographic indices (relief and elevation), cooling ages, and the structural cross section (Figure 3) are compared in Figure 11. Regions of young AHe and AFT ages ($<$3 Ma) and high exhumation rates ($\geq$1 mm/year) correspond with active structures in the Sub-Himalaya and the KW (Figures 11a and 11c). Precipitation reaches peak values (~4 m/year) on the south flank of the Pir Panjal Range and drop steadily northward to $\ll$1 m/year across the High Himalaya (Figure 11b). At the position of the KW, precipitation is ~1.5 m/year or less than half of the annual precipitation over the Sub-Himalaya (Figure 11b). Mean elevation and relief similarly increase northward, although the greatest relief corresponds to the KW and the Zanskar Range on the southern edge of the Tibetan Plateau marks the highest mean elevation. Young cooling ages in the Sub-Himalaya thus coincide with high annual precipitation, low mean elevation, and low relief. Comparably young ages within the KW are associated with lower annual precipitation but high relief and mean elevation. Thus, although the Pir Panjal Range represents

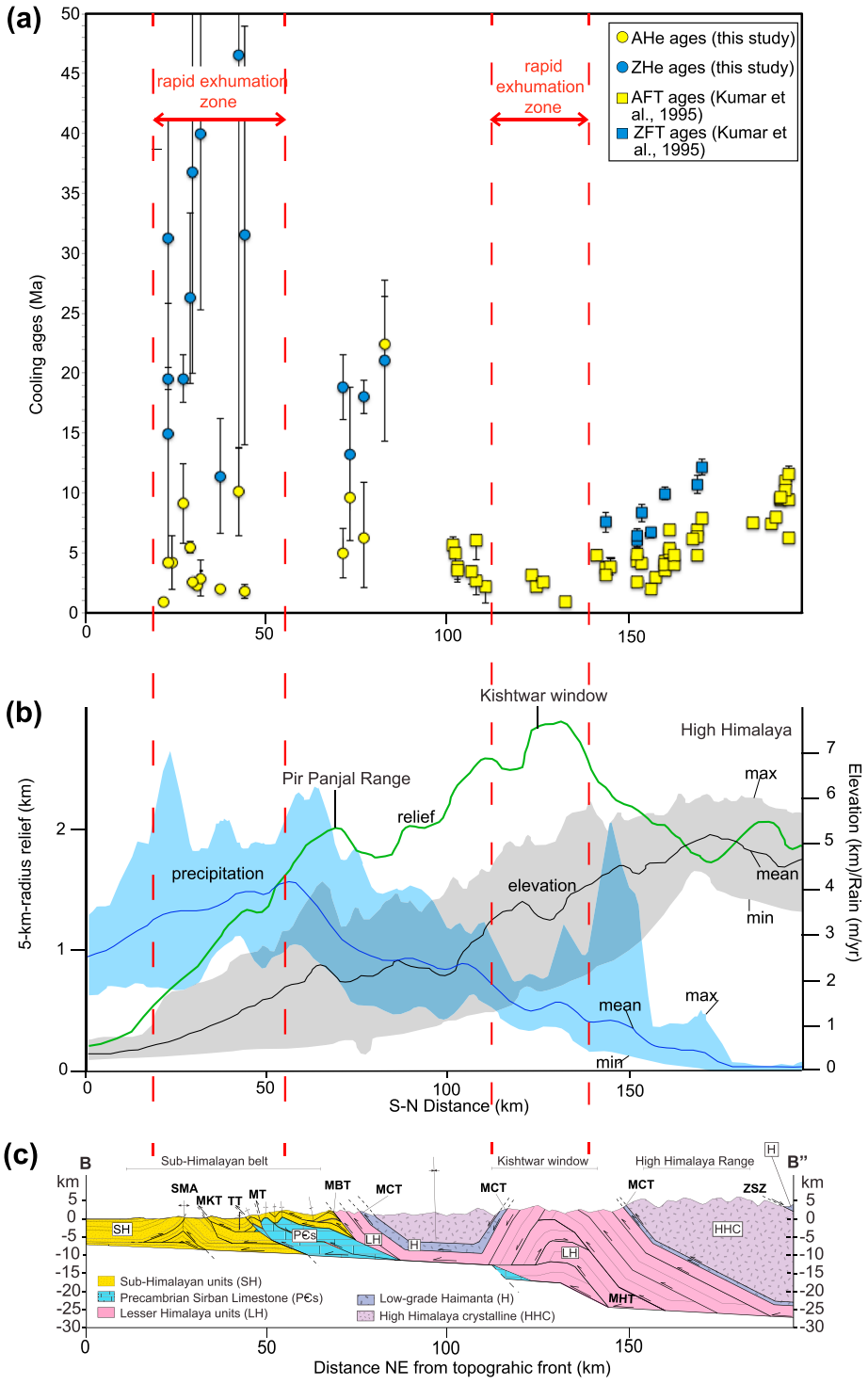

Figure 11. Data compilation of cooling ages, relief, precipitation, and simplified regional cross section from distance north of the axial trace of the frontal fold (Suruin-Mastgarh anticline) to the Zanskar Shear Zone. (a) Plot of AHe, ZHe ages (this study), and cited AFT and ZFT ages for the Kishtwar window and High Himalaya (Kumar et al., 1995). (b) Relief and precipitation swath (100 × 350 km) along the same transect location as the available regional cross section. The blue line indicates TRMM-derived rainfall, the black lines show mean elevation, and the green line denotes 5-km-radius relief from 90-m digital elevation model. Topographic and precipitation data taken from data repository in Bookhagen and Burbank (2006). The shaded outline for rainfall and elevation lines represent maximum and minimum envelopes around a mean. (c) Simplified SW-NE regional cross section along transect line B-B′-B″ from the Suruin-Mastgarh anticline (SMA) to the Zanskar Shear Zone (ZSZ) in the Kashmir Himalaya. See Figure 4 for location. Full name abbreviations listed in Figure 2.

a clear barrier that focuses orographic precipitation, cooling ages vary as a function of structural position within the orogen and independently of precipitation.

Along strike to the southeast, young AFT cooling ages (<3 Ma) and high exhumation rates (>1 mm/year) correspond with the southwestern flank of the Dhauladhar Range in Himachal Pradesh (Figures 4 and 9). The range is bounded by the MBT and MCT, but the hanging wall thrust sheet (the Chamba Nappe; Robyr et al., 2006) is not folded above a structural culmination as seen at the KW along strike to the northwest or the Rampur window along strike to the southeast (Figures 1 and 2). High orographic precipitation, increasing relief, and mean elevation also correspond with the southwestern flank of the range (Bookhagen & Burbank, 2006). Spatial correspondence between young cooling ages and high exhumation rates, high precipitation, and rising mean elevation leads Deeken et al. (2011) and Adlakha et al. (2013) to conclude that climate-enhanced exhumation focused deformation along the southwestern flank of the Dhauladhar Range. Alternatively, we argue that structurally driven orogenic growth along the MHT driving upper plate exhumation and tilting of the MBT and MCT thrust sheets can explain the same pattern of young cooling ages in the Dhauladhar Range. Such strong variability in along-strike exhumation and geometry of the MHT between the Kashmir Himalaya and neighboring ranges to the southeast is likely reflects lateral geometric variations in the MHT geometry. It is not clear what controls such lateral variation between the Kashmir Himalaya and Himachal Pradesh, given that no significant inherited basement cross-strike faults have been resolved for this area (e.g., Gahalaut & Kundu, 2012; Godin & Harris, 2014). Lateral variation in preorogenic basin fill thickness (Prasad et al., 2011) or a combination of the evolution ramp formation-advection system and the rheological contrast between colliding plate and Tibetan plateau may provide more suitable explanations (Mercier et al., 2017).

In the Kashmir Himalaya, exhumation rates do seem to vary as a function of the underlying structures. Exhumation rates are relatively high across the KW above the structural culmination and low over the neighboring across-strike klippe (Pir Panjal Range; Figure 3), as expected for structurally controlled variation in structural relief and shortening (Boyer & Elliott, 1982; DeCelles et al., 2001; DeCelles, Gehrels, Quade, & Ojha, 1998; Schelling & Arita, 1991). Thus, the anticorrelation between cooling ages, topography, and precipitation along the transect across the KW and their correspondence along the Chamba Nappe transect strongly suggests that along-strike changes in the thrust belt structural architecture control exhumation. Thrust ramps such as steps in the MHT and relatively small ramps in upper plate faults explain across-strike variation in uplift rate and exhumation both along the KW cross section (Figure 3) and regionally across the Salt Range thrust sheet in Pakistan (Burbank & Beck, 1989), the Himalayan frontal fault in India and Nepal (Lavé & Avouac, 2000; Wesnousky et al., 1999), and a MHT ramp thought to underlie the main topographic step between the Lesser and High Himalaya (Seeber et al., 1981; Bilham et al., 1997; Avouac, 2003; Schiffman et al., 2013).

7. Conclusion

Apatite and zircon (U-Th)/He cooling ages quantify the late Cenozoic exhumation pattern associated with fault activity across the Kashmir Himalaya. Utilizing new data in combination with published low-temperature thermochronologic data, we constrain the cooling history and thrust belt kinematics across an ~190-km section of the Kashmir Himalaya. AHe and ZHe samples were collected from folds and faults across the foreland in the Sub-Himalayan belt and from thrust sheets in the hinterland of the Pir Panjal Range. In the foreland, we interpret regional patterns of young AHe cooling ages (<4 Ma; Figure 4) as reset detrital cooling ages because they are younger than the sampled stratigraphic units (Figure 5a). Thermal models of the AHe data demonstrate that cooling associated with thrusting was underway by 4 Ma (Figure 8 and supporting information S1), and high exhumation rates (≥1 mm/year; Figure 9) are the result of thrust-related exhumation on structures within the Sub-Himalaya. Coeval distributed shortening across multiple faults in the Kashmir Sub-Himalaya explains the regional upper-plate exhumation and demonstrates that it was established since ~4 Ma. In the Kashmir Himalaya hinterland along the Pir Panjal Range, AHe data yield older cooling (> 5.1 Ma) and lower exhumation rates across the MBT and MCT (Figures 4 and 9). Hinterland and foreland ZHe age data reveal a similar cluster in cooling ages (14–23 Ma) associated with exhumation and erosion on the MCT. Further north in the hinterland, young AHe cooling ages (<3 Ma) and high exhumation rates (3.6–3.2 mm/year), ~100 km north of the active deformation front (Figures 4, 9, 10, 11) indicates that duplex growth

responsible for the KW accompanied accretion and deformation of the foreland (Figure 3). Distributed deformation across the foreland in concert with duplex growth in the hinterland suggests that a subcritical orogenic wedge characterizes the Kashmir Himalaya following accretion of the foreland since ~4 Ma. Decoupling of precipitation and Late Cenozoic cooling and exhumation in the Kashmir Himalaya suggests that climate is not the primary driver of deformation. Rather these new data indicate that the exhumation pattern since 4 Ma primarily reflects changes in structural architecture and spatial variability in the distribution of shortening.

Acknowledgments
This research was supported by the National Science Foundation grant EAR-0635987. The (U-Th)/He dating analyses were made possible by the collaboration of the University of Kansas He Lab and assistance of Charles Verdel. Fieldwork and logistics were facilitated by the collaborations and assistances of Idrees Bhat, Vikram Sharma, Shabir Ahmad, and M.I. Bhat at the University of Kashmir. Constructive reviews by Peter van der Beek, Devon Orme, and Associate Editor Virginia Toy help refine the presentation and interpretation of the data. We thank Editor John Geissman for his editorial handling. The data used are listed in the tables and supporting information.

References

Abrahami, R., van der Beek, P., Huyghe, H., Hardwick, E., & Carcaillet, J. (2016). Decoupling of long-term exhumation and short-term erosion rates in the Sikkim Himalaya. *Earth and Planetary Science Letters*, *433*, 76–88. https://doi.org/10.1016/j.epsl.2015.10.039

Adlakha, V., Patel, R. C., Lal, N., Metha, Y. P., Jain, A. K., & Kumar, A. (2013). Tectonics and climate interplay: Exhumation pattern of the Dhauladhar Range, Northwest Himalaya. *Current Science*, *104*(11), 1551–1559.

Agarwal, R. P., Prasad, D. N., Samanta, U., Berry, C. M., & Sharma, J. (1994). Hydrocarbon potential of Siwalik Basin. In *Siwalik Foreland Basin of Himalaya, Himalayan Geology, 15*, (pp. 301–320). Dehra Dun: Wadia Institute of Himalayan Geology.

Avouac, J. P. (2003). Mountain building, erosion and the seismic cycle in the Nepal Himalaya. *Advances in Geophysics*, *46*, 1–79. https://doi.org/10.1016/S0065-2687(03)46001-9

Avouac, J. P., Ayoub, F., Leprince, S., Konca, O., & Helmberger, D. V. (2006). The 2005, Mw 7.6 Kashimir earthquake: Sub-pixel correlation of ASTER images and seismic waveforms analysis. *EPSL*, *249*(3-4), 514–528. https://doi.org/10.1016/j.epsl.2006.06.025

Bernet, M., & Spiegel, C. (2004). Introduction: Detrital thermochronology. *Geological Society of America Special Papers*, *378*, 1–6.

Bhatia, T. R., & Bhatia, S. K. (1973). Sedimentology of the shale belt of Ramban-Banihal area. *Kashmir Himalaya, Himalayan Geology*, *3*, 116–134.

Bilham, R., Larson, K., & Freymueller, J. (1997). GPS measurements of present day convergence across the Nepal Himalaya. *Nature*, *386*(6620), 61–64. https://doi.org/10.1038/386061a0

Blythe, A. E., Burbank, D. W., Carter, A., Schmidt, K., & Putkonen, J. (2007). Plio-Quaternary exhumation history of the central Nepalese Himalaya: 1. Apatite and zircon fission-track and apatite [U-Th]/He analyses. *Tectonics*, *26*, TC3002. https://doi.org/10.1029/2006TC001990

Bollinger, L., Henry, P., & Avouac, J. P. (2006). Mountain building in the Himalaya: Thermal and kinematic model from 20 Ma to present. *Earth and Planetary Science Letters*, *224*, 58–71.

Bookhagen, B., & Burbank, D. W. (2006). Topography, relief, and TRMM-derived rainfall variations along the Himalaya. *Geophysical Research Letters*, *33*, L08405. https://doi.org/10.1029/2006GL026037

Bookhagen, B., & Burbank, D. W. (2010). Toward a complete Himalayan hydrological budget: Spatiotemporal distribution of snowmelt and rainfall and their impact on river discharge. *Journal of Geophysical Research*, *115*, F03019. https://doi.org/10.1029/2009JF001426

Boyer, S. E. (1992). Geometric evidence for synchronous thrusting in the southern Albert and northwest Montana thrust belts. In K. R. McClay (Ed.), *Thrust tectonics* (pp. 377–390). New York: Chapman and Hall.

Boyer, S. E. (1995). Sedimentary basin taper as a factor controlling the geometry and advance of thrust belts. *American Journal of Science*, *295*(10), 1220–1254. https://doi.org/10.2475/ajs.295.10.1220

Boyer, S. E., & Elliott, D. (1982). Thrust systems. *American Association of Petroleum Geologists Bulletin*, *66*, 1196–1230.

Brewer, I. A., & Burbank, D. (2006). Thermal and kinematic modeling of bedrock and detrital cooling ages in the Central Himalaya. *Journal of Geophysical Research*, *111*, B09409. https://doi.org/10.1029/2004JB003304

Brozovic, N., & Burbank, D. W. (2000). Dynamic fluvial systems and gravel progradation in the. *Geological Society of America Bulletin*, *112*(3), 394–412.

Burbank, D. W., & Beck, R. A. (1989). Early Pliocene uplift of the salt range: Temporal and constraints on thrust wedge development. In L. L. Malinconico, & R. J. Lillie (Eds.), *Tectonics of the Western Himalaya, volume special paper 232* (pp. 113–128). Boulder, CO: Geological Society of America.

Burbank, D. W., Beck, R. A., & Mulder, T. (1996). The Himalayan Foreland Basin. In A. Yin, & M. Harrison (Eds.), *The tectonic evolution of Asia* (pp. 149–190). Cambridge: Cambridge University Press.

Burbank, D. W., Blythe, A. E., Putkonen, J., Pratt-Sitaula, B., Gabet, E., Oskin, M., et al. (2003). Decoupling of erosion and precipitation in the Himalayas. *Nature*, *426*(6967), 652–655. https://doi.org/10.1038/nature02187

Burbank, D. W., Vergés, J., & MuÒoz, J. A. (1992). Coeval hindward- and forward-imbricating thrusting in the central southern Pyrenees: Timing and rates of shortening and deposition. *Geological Society of America Bulletin*, *104*, 1–18.

Catlos, E., Harrison, T. M., Manning, C. E., Grove, M., Rai, S. M., Hubbard, M. S., & Upreti, B. (2002). Records of the evolution of the Himalayan orogen from in situ Th–Pb ion microprobe dating of monazite: Eastern Nepal and western Garhwal. *Journal of Asian Earth Sciences*, *20*(5), 459–479.

Cerveny, P. F., Naeser, N. D., Zeitler, P. K., Naeser, C. W., & Johnson, N. M. (1988). History of uplift and relief of the Himalaya during the past 18 million years; evidence from sandstones of the Siwalik Group. In K. L. Kleinspehn & C. Paola (Eds.), *New perspectives in basin analysis* (pp. 43–61). New York: Springer-Verlag.

Dahlen, F. A., & Suppe, J. (1988). Mechanics, growth, and erosion of mountain belts. In S. P. Clark, B. C. Burchfiel, & J. Suppe (Eds.), *Processes in continental lithospheric deformation, Geological Society of America Special Paper* (Vol. 218, pp. 161–178). https://doi.org/10.1130/SPE218-p161

Dahlstrom, C. D. A. (1969). Balanced cross sections. *Canadian Journal of Earth Sciences*, *6*(4), 743–757. https://doi.org/10.1139/e69-069

Davis, D., Suppe, J., & Dahlen, F. A. (1983). Mechanics of fold-and thrust belts and accretionary wedges. *Journal of Geophysical Research*, *88*(B2), 1153–1172. https://doi.org/10.1029/JB088iB02p01153

Davis, E. E., & Hyndman, R. D. (1989). Accretion and recent deformation of sediments along the northern Cascadia subduction zone. *Geological Society of America Bulletin*, *101*(11), 1465–1480. https://doi.org/10.1130/0016-7606(1989)101<1465:AARDOS>2.3.CO;2

DeCelles, P. G., & Coogan, J. C. (2006). Regional structure and kinematic history of the Sevier fold-and-thrust belt, central Utah. *Geological Society of America Bulletin*, *118*(7–8), 841–864. https://doi.org/10.1130/B25759.1

DeCelles, P. G., Gehrels, G. E., Quade, J., & Ojha, T. P. (1998). Eocene–early Miocene foreland basin development and the history of the Himalayan thrusting, western and central Nepal. *Tectonics*, *17*(5), 741–765. https://doi.org/10.1029/98TC02598

DeCelles, P. G., Gehrels, G. E., Quade, J., Ojha, T. P., & Kapp, P. A. (1998). Neogene foreland basin deposits, erosional unroofing and the kinematic history of the Himalayan fold-thrust belt, western Nepal. *Geological Society of America Bulletin*, *110*(1), 2–21. https://doi.org/10.1130/0016-7606(1998)110<0002:NFBDEU>2.3.CO;2

DeCelles, P. G., & Mitra, G. (1995). History of northeast Utah Sevier orogenic wedge in terms of critical taper models, Geological Society of America, Rocky Mtn. Section, Abstracts with Programs, 27, no. 4, p. 8.

DeCelles, P. G., Robinson, D. M., Quade, J., Ojha, T. P., Garzione, C. N., Copeland, P., & Upreti, B. N. (2001). Stratigraphy, structure, and tectonic evolution of the Himalayan fold-thrust belt in western Nepal. *Tectonics*, *20*(4), 487–509. https://doi.org/10.1029/2000TC001226

Deeken, A., Thiede, R. C., Sobel, E. R., Hourigan, J. K., & Strecker, M. R. (2011). Exhumational variability within the Himalaya of northwest India. *Earth Planetry Science Letters*, *305*(1-2), 103–114. https://doi.org/10.1016/j.epsl.2011.02.045

DiPietro, J. A., & Pogue, K. R. (2004). Tectonostratographic subdivisions of the Himalaya. *Tectonics*, *23*, TC5001. https://doi.org/10.1029/2003TC001554

Dodson, M. H. (1973). Closure temperature in cooling geochronological and petrological systems. *Contributions to Mineralogy and Petrology*, *40*(3), 259–274. https://doi.org/10.1007/BF00373790

Ehlers, T. A., & Farley, K. A. (2003). Apatite (U-Th)/He thermochronometry: Methods and applications to problems in tectonic and surface processes. *Earth and Planetary Science Letters*, *206*, –1, 14.

Farley, K. A., & Stockli, D. F. (2002). (U-Th)/He dating of phosphates: Apatite, monazite, and xenotime. In M. Kohn, J. Rakovan, & J. M. Hughes (Eds.), *Phosphates, Rev. Mineral* (Vol. 15, pp. 559–578). Washington, DC: Mineral. Soc. Am.

Flowers, R. M., Farley, K. A., & Ketcham, R. A. (2015). A reporting protocol for thermochronologic modeling illustrated with data from the Grand Canyon. *Earth and Planetary Science Letters*, *432*, 425–435. https://doi.org/10.1016/j.epsl.2015.09.053

Flowers, R. M., Ketcham, R. A., Shuster, D. L., & Farley, K. A. (2009). Apatite (U-Th)/He thermochronometry using a radiation damage accumulation and annealing model. *Geochimica et Cosmochimia Acta*, *73*(8), 2347–2365. https://doi.org/10.1016/j.gca.2009.01.015

Frank, W., Grasemann, B., Guntli, P., & Miller, C. (1995). Geological map of the Kishtwar-Chamba-Kulu region (NWHimalaya India). *Jahrbuch der Geologischen Bundesanstalt*, *138*(2), 299–308.

Gahalaut, V. K., & Kundu, B. (2012). Possible influence of subducting ridges on the Himalayan arc and on the ruptures of great and major Himalayan earthquakes. *Gondwana Research*, *21*(4), 1080–1088. https://doi.org/10.1016/j.gr.2011.07.021

Gallagher, K. (2012). Transdimensional inverse thermal history modeling for quantitative thermochronology. *Journal of Geophysical Research*, *117*, B02408. https://doi.org/10.1029/2011JB008825

Gavillot, Y., Axen, A. J., Stockli, D. F., Horton, B. K., & Fakhari, M. (2010). Timing of thrust activity in the High Zagros fold-thrust belt, Iran, from (U-Th)/He thermochronometry. *Tectonics*, *29*, TC4025. https://doi.org/10.1029/2009TC002484

Gavillot, Y., Meigs, A., Yule, Y., Heermance, R., Rittenour, T., Madugo, C., & Malik, M. (2016). Shortening rate and Holocene surface rupture on the Riasi fault system in the Kashmir Himalaya: Active thrusting within the Northwest Himalayan orogenic wedge. *Geological Society of America Bulletin*, *128*(7-8), 1070–1094. https://doi.org/10.1130/B31281.1

Gavillot, Y. G. (2014). Active tectonics and earthquake potential on folds, out-of-sequence thrusts, and duplexes in the Kashmir Himalaya (NW India) (PhD thesis): Corvallis, Oregon, Oregon State University, 231 p.

Gavillot, Y. G., Meigs, A. M., Hebeler, A. H., Yule, D., Madden, C., Malik, M. M., & Kaericher, M. K. (2010). Active thrusting within the Himalayan orogenic wedge in the Kashmiri Himalaya. *Seismological Research Letters*, *81*(2), –325.

Gilluly, J. (1960). A folded thrust in Nevada-inferences as to time relations between folding and faulting. *American Journal of Science*, *258*, 68–79.

Gleadow, A. J. W., & Fitzgerald, P. G. (1987). Tectonic history and structure of the Transantarctic Mountains: New evidence from fission track dating in the Dry Valleys area of southern Victoria Land. *Earth and Planetary Science Letters*, *82*(1-2), 1–14. https://doi.org/10.1016/0012-821X(87)90102-6

Godin, L., & Harris, L. B. (2014). Tracking basement cross-strike discontinuities in the Indian crust beneath the Himalayan orogen using gravity data - relationship to upper crustal faults. *Geophysical Journal International*, *198*(1), 198–215. https://doi.org/10.1093/gji/ggu131

Griesbach, C. L. (1891). Geology of the Central Himalayas. *Memoirs - Geological Survey of India*, *23*, 1–232.

Grujic, D., Coutand, I., Bookhagen, B., Bonnet, S., Blythe, A., & Duncan, C. (2006). Climatic forcing of erosion, landscape, and tectonics in the Bhutan Himalayas. *Geology*, *34*(10), 801–804. https://doi.org/10.1130/G22648.1

Guenthner, W. R., Reiners, P. W., Ketcham, R. A., Nasdala, L., & Giester, G. (2013). Helium diffusion in natural zircon: Radiation damage, anisotropy, and the interpretation of zircon (U-Th)/He thermochronology. *American Journal of Science*, *313*(3), 145–198. https://doi.org/10.2475/03.2013.01

Gutscher, M.-A., Kukowski, N., Malavieille, J., & Lallemand, S. (1996). Cyclical behavior of thrust wedges: Insights from high basal friction sandbox experiments. *Geology*, *24*(2), 135–138. https://doi.org/10.1130/0091-7613(1996)024<0135:CBOTWI>2.3.CO;2

Gutscher, M.-A., Kukowski, N., Malavieille, J., & Lallemand, S. (1998). Episodic imbricate thrusting and underthrusting: Analog experiments and mechanical analysis applied to the Alaskan Accretionary Wedge. *Journal of Geophysical Research*, *103*(B5), 10,161–10,176. https://doi.org/10.1029/97JB03541

Herman, F., Copeland, P., Avouac, J. P., Bollinger, L., Maheo, G., Le Fort, P., et al. (2010). Exhumation, crustal deformation, and thermal structure of the Nepal Himalaya derived from the inversion of thermochronological and thermobarometric data and modeling of the topography. *Journal of Geophysical Research*, *115*, B06407. https://doi.org/10.1029/2008JB006126

Hodges, K., Wobus, C. W., Ruhl, K., Schildgen, T., & Whipple, K. (2004). Quaternary deformation, river steepening, and heavy precipitation at the front of the Higher Himalayan ranges. *Earth and Planetary Science Letters*, *220*(3-4), 379–389. https://doi.org/10.1016/S0012-821X(04)00063-9

Hodges, K. V. (2000). Tectonics of the Himalaya and Tibet from two perspectives. *Geological Society of America Bulletin*, *112*(3), 324–350. https://doi.org/10.1130/0016-7606(2000)112<324:TOTHAS>2.0.CO;2

Hodges, K. V., Hurtado, J. M., & Whipple, K. X. (2001). Southward extrusion of Tibetan crust and its effect on Himalayan tectonics. *Tectonics*, *20*(6), 799–809. https://doi.org/10.1029/2001TC001281

Hoth, S., Adam, J., Kukowski, N., & Oncken, O. (2006). Influence of erosion on the kinematics of bivergent orogens: Results from scaled sandbox simulations. *Geological Society of America Special Papers*, *398*, 201–225. https://doi.org/10.1130/2006.2398(12)

Hoth, S., Hoffmann-Rothe, A., & Kukowski, N. (2007). Frontal accretion: An internal clock for bivergent wedge deformation and surface uplift. *Journal of Geophysical Research*, *112*, B06408. https://doi.org/10.1029/2006JB004357

Huntington, K. W., & Hodges, K. V. (2006). A comparative study of detrital mineral and bedrock age-elevation methods for determining erosion rates. *Journal of Geophysical Research*, *111*, FO3011. https://doi.org/10.1029/2005JF000454

Hussain, A., Yeats, R. S., & MonaLisa (2009). Geological setting of the 8 October 2005 Kashmir earthquake. *Journal of Seismology*, *13*(3), 315–325. https://doi.org/10.1007/s10950-008-9101-7

Hussain, S. H., Haq, I., & Hussain, A. (2004). Geological map of the Khuiratta area, District Kotli, AJK: Geol. Survey of Pakistan Geological Map Series v, VI, no. 27, Sheet No.43 K/3, 1:50,000.
Iqbal, S., Nasir, S., & Hussain, A. (2004). Geological map of the Nauseri area, District Muzaffarabad, AJK, Geol. Survey of Pakistan Geological Map Series v. VI, no. 14, Sheet No. 43 F/11, 1:50,000.
Jain, A. K., Kumar, D., Singh, S., Kumar, A., & Lal, N. (2000). Timing, quantification and tectonic modelling of Pliocene–Quaternary movements in the NW Himalaya: Evidence from fission track dating. *Earth Planetry Science Letters*, *179*(3-4), 437–451. https://doi.org/10.1016/S0012-821X(00)00133-3
Ji, C., Helmberger, D. V., Song, A. T.-R., Ma, K.-F., & Wald, D. J. (2001). Slip distribution and tectonic implications of the 1999 Chi-Chi, Taiwan earthquake. *Geophysical Research Letters*, *28*(23), 4379–4382. https://doi.org/10.1029/2001GL013225
Jordan, T. E., Allmendinger, R. W., Damanti, J. F., & Drake, R. E. S. S. B. A. A. (1993). Chronology of motion in a complete thrust belt: The Precordillera, 30–31°S, Andes Mountains. *Journal of Geology*, *101*(2), 135–156.
Kaneda, H., Nakata, T., Tsutsumi, H., Kondo, H., Sugito, N., Awata, Y., et al. (2008). Surface rupture of the 2005 Kashmir, Pakistan, Earthquake and its Active Tectonic Implications. *Bulletin of the Seismological Society of America*, *98*(2), 521–557. https://doi.org/10.1785/0120070073
Karunakaran, C., & Ranga Rao, A. (1976). *Status of exploration for hydrocarbons in the Himalayan region—Contributions to stratigraphy and structure* (pp. 1–72). Himalayan Geology Seminar: New Delhi.
Ketcham, R. A., Donelick, R. A., & Carlson, W. D. (1999). Variability of apatite fission-track annealing kinetics: III. Extrapolation to geological time scales. *American Mineralogist*, *84*(9), 1235–1255.
Kondo, H., Nakata, T., Akhtar, S. S., Wesnousky, S. G., Sugito, N., Kaneda, H., et al. (2008). Long recurrence interval of faulting beyond the 2005 Kashmir earthquake around the northwestern margin of the Indo-Asian collision zone. *Geology*, *36*(9), 731–734. https://doi.org/10.1130/G25028A.1
Kumar, A., Lal, N., Jain, A. K., & Sorkhabi, R. B. (1995). Late Cenozoic–Quaternary thermo- tectonic history of Higher Himalayan Crystalline (HHC) in Kishtwar–Padar–Zanskar region, NW Himalaya: Evidence from fission-track ages. *Journal of the Geological Society of India*, *45*(4), 375–391.
Kumar, R., Ghosh, S. K., Mazari, R. K., & Sangode, S. J. (2003). Tectonic impact on the fluvial deposits of Plio-Pleistocene Himalayan foreland basin. *Sedimentary Geology*, *158*(3-4), 209–234. https://doi.org/10.1016/S0037-0738(02)00267-1
Kumar, S., Wesnousky, S. G., Rockwell, T. K., Briggs, R. W., Thakur, V. C., & Jayangondaperumal, R. (2006). Paleoseismic evidence of great surface rupture earthquakes along the Indian Himalaya. *Journal of Geophysical Research*, *111*, B03304. https://doi.org/10.1029/2004JB003309
Kumaravel, V., Sangode, S. J., Kumar, R., & Siva Siddaiah, N. (2005). Magnetic polarity stratigraphy of Plio-Pleistocene Pinjor formation (type locality), Siwalik group, NW Himalaya, India. *Current Science*, *88*, 1453–1461.
Lal, N., Mehta, Y. D., Kumar, D., Kumar, A., & Jain, A. K. (1999). Cooling and exhumation history of the Mandi granite and adjoining tectonic units, Himachal Pradesh, and estimation of closure temperature from external surface of zircon. In A. K. Jain, & R. M. Manickavasagam (Eds.), *Geodynamic of the NW Himalaya* (pp. 207–216). Osaka, Japan: Gondwana Research Group.
Landry, K. R., Coutand, I., Whipp, D. M. Jr., Grujic, D., & Hourigan, J. K. (2016). LateNeogene tectonically driven crustalexhumation of the Sikkim Himalaya: Insights from inversion of multithermo-chronologic data. *Tectonics*, *35*, 833–859. https://doi.org/10.1002/2015TC004102
Lavé, J., & Avouac, J. P. (2000). Active folding of fluvial terraces across the Siwaliks Hills, Himalayas of central Nepal. *Journal of Geophysical Research*, *105*(B3), 5735–5770. https://doi.org/10.1029/1999JB900292
Lavé, J., Yule, D., Sapkota, S., Basant, K., Madden, C., Attal, M., & Pandey, R. (2005). Evidence for a great Medieval earthquake (~1100 A.D.) in the central Himalayas, Nepal. *Science*, *307*(5713), 1302–1305. https://doi.org/10.1126/science.1104804
Lee, J.-C., Chen, Y.-G., Sieh, K., Mueller, K., Chen, W.-S., Chu, H.-T., et al. (2001). A vertical exposure of the 1999 surface rupture of the Chelungpu Fault at Wufeng, western Taiwan: Structural and paleoseismic implications for an active thrust fault. *Bulletin of the Seismological Society of America*, *91*(5), 914–929.
Meigs, A. J., & Burbank, D. W. (1997). Growth of the south Pyrenean orogenic wedge. *Tectonics*, *16*(2), 239–258. https://doi.org/10.1029/96TC03641
Meigs, A. J., Burbank, D. W., & Beck, R. A. (1995). Middle-late Miocene (>10 Ma) formation of the Main Boundary Thrust in the western Himalaya. *Geology*, *23*(5), 423–426. https://doi.org/10.1130/0091-7613(1995)023<0423:MLMMFO>2.3.CO;2
Mercier, J., Braun, J., & van der Beek, P. (2017). Do along-strike tectonic variations in the Nepal Himalaya reflect different stages in the accretion cycle? Insights from numerical modeling. *Earth Planetry Science Letters*, *472*, 299–308. https://doi.org/10.1016/j.epsl.2017.04.041
Metcalfe, R. (1993). Pressure, temperature and time constraints on metamorphism across the Main Central Thrust zone and High Himalayan Slab in the Garhwal Himalaya. *Geological Society, London, Special Publications*, *74*(1), 485–509. https://doi.org/10.1144/GSL.SP.1993.074.01.33
Molnar, P., & Lyon-Caen, H. (1988). Some simple physical aspects of the support, structure, and evolution of mountain belts, in Processes in continental lithospheric deformation. *Geological Society of America Special Papers*, *218*, 179–207.
MonaLisa, Khwaja, A. A., Qasim Jan, M., Yeats, R. S., Hussain, A., & Khan, S. A. (2009). New data on the Indus Kohistan seismic zone and its extension into the Hazara-Kashmir syntaxis, NW Himalayas of Pakistan. *Journal of Seismology*, *13*(3), 339–361. https://doi.org/10.1007/s10950-008-9117-z
Morley, C. (1988). Out-of-sequence thrusts. *Tectonics*, *7*(3), 539–561. https://doi.org/10.1029/TC007i003p00539
Mugnier, J.-L., Huyghe, P., Leturmy, P., & Jouanne, F. (2004). Episodicity and rates of thrust-sheet motion in the Himalayas (Western Nepal), in McClay, K.R., ed., Thrust Tectonics and Hydrocarbon Systems. *AAPG Memoir*, *82*, 91–114.
Mugnier, J.-L., Leturmy, P., Mascle, G., Huyghe, P., Chalaron, E., Vidal, G., et al. (1999). The Siwaliks of western Nepal I. Geometry and kinematics. *Journal of Asian Earth Sciences*, *17*(5-6), 629–642. https://doi.org/10.1016/S1367-9120(99)00038-3
Nakata, T. (1989). Active faults of the Himalaya of India and Nepal. In L. L. Malinconinco, Jr. & R. J. Lillie (Eds.), *Tectonics of the Western Himalayas* (pp. 243–264). Boulder, CO: Geological Society of America.
Norris, R. J., & Cooper, A. F. (1997). Erosional control on the structural evolution of a transpressional thrust complex on the Alpine Fault, New Zealand. *Journal of Structural Geology*, *19*(10), 1323–1342. https://doi.org/10.1016/S0191-8141(97)00036-9
Oriel, S. S. (1950). *Geology and mineral resources of the hot springs window*. Madison County, North Carolina, North Carolina: Department of Conservation and Development.
Patel, R. C., & Carter, A. (2009). Exhumation history of the Higher Himalayan crystalline along Dhauliganga-Goriganga river valleys, NW India: New constraints from fission track analysis. *Tectonics*, *28*, TC3004. https://doi.org/10.1029/2008TC002373
Prasad, B. R., Klemperer, S. L., Rao, V. V., Tewari, H. C., & Khare, P. (2011). Crustal structure beneath the Sub-Himalayan fold-thrust belt, Kangra recess, northwest India, from seismic reflection profiling: Implications for Late Paleoproterozoic orogenesis and modern earthquake hazard. *Earth and Planetary Science Letters*, *308*(1–2), 218–228. https://doi.org/10.1016/j.epsl.2011.05.052

Powers, P. M., Lillie, R. J., & Yeats, R. S. (1998). Structure and shortening of the Kangra and Dehra Dun reentrants, Sub-Himalaya, India. *Geological Society of America Bulletin*, *110*(8), 1010–1027. https://doi.org/10.1130/0016-7606(1998)110<1010:SASOTK>2.3.CO;2

Price, R. A. (1981). The Cordilleran foreland thrust and fold belt in the southern Canadian Rocky Mountains. In K. R. McClay, & N. J. Price (Eds.), *Thrust and Nappe tectonics, Volume Geological Society of London Special Publications 9* (pp. 427–448). London: Geological Society of London.

Rahn, M. K., Brandon, M. T., Batt, G. E., & Garver, J. I. (2004). A zero-damage model for fission- track annealing in zircon. *American Mineralogist*, *89*(4), 473–484. https://doi.org/10.2138/am-2004-0401

Raiverman, V., Kunte, S. V., & Mukherjea, A. (1983). Basin geometry, Cenozoic sedimentation and hydro-carbon prospects in North Western Himalaya and Indo-Gangetic plains. *Petroleum Asia Journal*, *6*, 67–92.

Ranga Rao, A., Agarwal, R. P., Sharma, U. N., Bhalla, M. S., & Nanda, A. C. (1988). Magnetic polarity stratigraphy and vertebrate paleontology of the Upper Siwalik Subgroup of Jammu Hills, India. *Journal of the Geological Society of India*, *31*, 361–385.

Ranga Rao, A., & Datta, N. K. (1976). Geological map of the Himalayan foot-hills. In C. Karunakaran & A. Ranga Rao (Eds.), *Himalayan geology seminar*. New Delhi, India: Section III: Oil and Natural Gas Resources, Oil and Natural Gas Commission. Sheet A, scale 1:300,000

Reiners, P. W. (2005). Zircon (U-Th)/He thermochronometry. In P. W. Reiners & T. A. Ehlers (Eds.), *Low-temperature thermochronology: Techniques, interpretations, and applications, Rev. Mineral. Geochem* (Vol. 58, pp. 151–179). Chantilly, VA: Mineral. Soc. of Am.

Reiners, P. W., Spell, T. L., Nicolescu, S., & Zanetti, K. A. (2004). Zircon (U–Th)/He thermochronometry: He diffusion and comparisons with $^{40}Ar/^{39}Ar$ dating. *Geochimica et Cosmochimica Acta*, *68*(8), 1857–1887. https://doi.org/10.1016/j.gca.2003.10.021

Robert, X., van der Beek, P., Braun, J., Perry, C., Dubille, M., & Mugnier, J.-L. (2009). Assessing Quaternary reactivation of the Main Central thrust zone (central Nepal Himalaya): New thermochronologic data and numerical modeling. *Geology*, *37*(8), 731–734. https://doi.org/10.1130/G25736A.1

Robyr, M., Hacker, B. R., & Mattison, J. M. (2006). Doming in compressional orogenic settings: New geochronological constraints from the NW Himalaya. *Tectonics*, *25*, TC2007. https://doi.org/10.1029/2004TC001774

Sangode, S. J., & Kumar, R. (2003). Magnetostratigraphic correlation of the Late Cenozoic fluvial sequences from NW Himalaya, India. *Current Science*, *84*(8), 1014–1024.

Sapkota, S. N., Bollinger, L., Klinger, Y., Tapponnier, P., Gaudemer, Y., & Tiwari, D. (2013). Primary surface ruptures of the great Himalayan earthquakes in 1934 and 1255. *Nature Geoscience*, *6*, 71–76.

Schelling, D., & Arita, K. (1991). Thrust tectonics, crustal shortening, and the structure of the far-eastern Nepal Himalaya. *Tectonics*, *10*(5), 851–862. https://doi.org/10.1029/91TC01011

Schiffman, C., Bali, B. S., Szeliga, W., & Bilham, R. (2013). Seismic slip deficit in the Kashmir Himalaya from GPS observations. *Geophysical Research Letters*, *40*, 5642–5645. https://doi.org/10.1002/2013GL057700

Schlup, M., Carter, A., Cosca, M., & Steck, A. (2003). Exhumation history of eastern Ladakh revealed by Ar-40/Ar-39 and fission-track ages: The Indus River-Tso Morari transect, NW Himalaya. *Journal of the Geological Society*, *160*(3), 385–399. https://doi.org/10.1144/0016-764902-084

Searle, M. P., & Godin, L. (2003). The South Tibetan Detachment and the Manaslu Leucogranite: A structural reinterpretation and restoration of the Annapurna-Manaslu Himalaya, Nepal. *Journal of Geology*, *111*(5), 505–523. https://doi.org/10.1086/376763

Searle, M. P., Stephenson, B., Walker, J., & Walker, C. (2007). Restoration of the Western Himalaya: Implications for metamorphic protoliths, thrust and normal faulting, and channel flow models. *Episodes*, *30*(4), 242–257.

Seeber, L., Armbruster, J. G., & Quittmeyer, R. C. (1981). Seismicity and continental subduction in the Himalayan arc, in Gupta, H.K., and Delany, F.M., eds., Zagros, Hindu-Kush Himalaya, geodynamic evolution. *American Geophysical Union Geodynamic Monograph*, *3*, 215–242. https://doi.org/10.1029/GD003p0215

Shah, S. M. I. (2009). Stratigraphy of Pakistan. *Geological Society of Pakistan Memoirs*, *22*, 291–299.

Sousa, F. J., Farley, K. A., Saleeby, J., & Clark, M. (2016). Eocene activity on the Western Sierra Fault System and its role incising Kings Canyon, California. *Earth and Planetary Science Letters*, *439*, 29–38. https://doi.org/10.1016/j.epsl.2016.01.020

Sousa, F. J., Saleeby, J., Farley, K. A., Unruh, J. R., & Lloyd, M. K. (2017). The southern Sierra Nevada pediment, central California. *Geosphere*, *13*(1), 82–101. ISSN 1553-040X, DOI: https://doi.org/10.1130/GES01369.1

Stephenson, B. J., Waters, D. J., & Searle, M. P. (2000). Inverted metamorphism and the Main Central Thrust: Field relations and thermo-barometric constraints from the Kishtwar window, NW Indian Himalaya. *Journal of Metamorphic Geology*, *18*(5), 571–590. https://doi.org/10.1046/j.1525-1314.2000.00277.x

Stockli, D. F. (2005). Application of low-temperature thermochronology to extensional tectonic settings. In P. W. Reiners, & T. A. Ehlers (Eds.), *Low-temperature thermochronology: Techniques, interpretations, and applications, Rev. Mineral. Geochem*., (Vol. 58, pp. 411–448). Chantilly, VA: Mineral. Soc. of Am.

Stockli, D. F., Farley, K. A., & Dumitru, T. A. (2000). Calibration of the (U-Th)/He thermochronometer on an exhumed normal fault block in the White Mountains, eastern California and western Nevada. *Geology*, *28*(11), 983–986. https://doi.org/10.1130/0091-7613

Stübner, K., Grujic, D., Dunkl, I., Thiede, R., & Eugster, P. (2018). Pliocene episodic exhumation and the significance of the Munsiari thrust in the northwestern Himalaya. *Earth and Planetary Science Letters*, *481*, 273–283. https://doi.org/10.1016/j.epsl.2017.10.036

Suppe, J. (1983). Geometry and kinematics of fault-propagation folding. *American Journal of Science*, *283*(7), 684–721. https://doi.org/10.2475/ajs.283.7.684

Tagami, T., Carter, A., & Hurford, A. J. (1996). Natural long-term annealing of the zircon fission- track system in Vienna Basin deep borehole samples: Constraints upon the partial annealing zone and closure temperature. *Chemical Geology*, *130*(1-2), 147–157. https://doi.org/10.1016/0009-2541(96)00016-2

Tagami, T., & Dumitru, T. A. (1996). Provenance and thermal history of the Franciscan accretionary complex: Constraints from fission track thermochronology. *Journal of Geophysical Research*, *101*(B5), 11,353–11,364. https://doi.org/10.1029/96JB00407

Tagami, T., Farley, K. A., & Stockli, D. F. (2003). Thermal sensitivities of zircon (U-Th)/He and fission-track systems. *Geochimica et Cosmochimica Acta*, *67*(18), 466.

Tagami, T., Galbraith, R. F., Yamada, R., & Laslett, G. M. (1998). Revised annealing kinetics of fission-tracks in zircon and geological implications. In P. Van den Haute & F. De Corte (Eds.), *Advances in fission-track geochronology* (pp. 99–112). New York: Springer.

Thakur, V. C. (1992). *Geology of Western Himalaya* (p. 363). Pergamon, Oxford: Pergamon Press.

Thakur, V. C. (1998). Structure of the Chamba nappe and position of the Main Central Thrust in Kashmir Himalaya. *Journal of Asian Earth Sciences*, *16*(2-3), 269–282. https://doi.org/10.1016/S0743-9547(98)00011-7

Thakur, V. C., Jayangondaperumal, R., & Malik, M. A. (2010). Redefining Medlicott Wadia's main boundary fault from Jhelum to Yamuna: An active fault strand of the Main Boundary thrust in northwest Himalaya. *Tectonophysics*, *489*(1-4), 29–42. https://doi.org/10.1016/j.tecto.2010.03.014

Thakur, V. C., & Rawat, B. S. (1992). *Geologic map of Western Himalaya, 1:1,000,000*. Dehra Dun, India: Wadia Institute of Himalayan Geology.

Thiede, R., Robert, X., Stübner, K., Dey, S., & Faruhn, J. (2018). ERRATUM: Sustained out-of-sequence shortening along a tectonically active segment of the Main Boundary thrust: The Dhauladhar Range in the northwestern Himalaya. *Lithosphere*, *10*(4), 579. https://doi.org/10.1130/L630E.1

Thiede, R. C., Bookhagen, B., Arrowsmith, J. R., Sobel, E. R., & Strecker, M. R. (2004). Climatic control on rapid exhumation along the southern Himalayan Front. *Earth and Planetary Science Letters*, *222*(3-4), 791–806. https://doi.org/10.1016/j.epsl.2004.03.015

Thiede, R. C., Arrowsmith, J. R., Bookhagen, B., McWilliams, M. O., Sobel, E. R., & Strecker, M. R. (2005). From tectonically to erosionally controlled development of the Himalayan orogeny. *Geology*, *33*(8), 689–692. https://doi.org/10.1130/G21483.1

Thiede, R. C., Ehlers, T. A., Bookhagen, B., & Strecker, M. R. (2009). Erosional variability along the northwest Himalaya. *Journal of Geophysical Research*, *114*, F01015. https://doi.org/10.1029/2008JF001010

Valdiya, K. S. (1998). *Dynamic Himalaya* (–178). India: Universities Press Hyderabad.

van der Beek, P., Camille, L., Baudin, M., Mercier, J., Robert, X., & Hardwick, E. (2016). Contrasting tectonically driven exhumation and incision patterns, western versus central Nepal Himalaya. *Geology*, *44*(4), 327–330. https://doi.org/10.1130/G37579.1

van der Beek, P., Robert, X., Mugnier, J.-L., Bernet, M., Huyghe, P., & Labrin, E. (2006). Late Miocene-Recent exhumation of the central Himalaya and recycling in the foreland basin assessed by apatite fission-track thermochronology of Siwalik sediments, Nepal. *Basin Research*, *18*(4), 413–434. https://doi.org/10.1111/j.1365-2117.2006.00305.x

Vannay, J. C., Grasemann, B., Rahn, M., Frank, W., Carter, A., & Baudraz, V. (2004). Miocene to Holocene exhumation of metamorphic crustal wedges in the Himalayan orogen: Evidence for tectonic extrusion coupled to fluvial erosion. *Tectonics*, *23*, TC1014. https://doi.org/10.1029/2002TC001429

Vassallo, R., Mugnier, J.-L., Vignon, V., Malik, M. A., Jayangondaperumal, R., Srivastava, P., et al. (2015). Distribution of the late-Quaternary deformation in northwestern Himalaya. *Earth and Planetary Science Letters*, *411*, 241–252. https://doi.org/10.1016/j.epsl.2014.11.030

Vergés, J., & Burbank, D. W. (1996). In P. F. Friend, & C. J. Dabrio (Eds.), *Eocene-Oligocene thrusting and basin configuration in the eastern and central Pyrenees (Spain)* (pp. 120–133). Tertiary basins of Spain: Cambridge University Press.

Vergés, J., & Muñoz, J. A. (1990). Thrust sequences in the southern central Pyrenees. *Bulletin de la Société Géologique de France*, *8*, 265–271.

Vermeesch, P., & Tian, Y. (2014). Thermal history modeling: HeFTy vs. QTQt. *Earth Science Reviews*, *139*, 279–290. https://doi.org/10.1016/j.earscirev.2014.09.010

Vignon, V. (2011). Activité hors séquence des chevauchements dans la syntaxe nord-ouest himalayenne: apports de la modélisation analogique et quantification quaternaire par analyse morphotectonique, PhD thesis, Université de Grenoble, France.

von Huene, R., & Scholl, D. W. (1991). Observations at convergent margins concerning sediment subduction, subduction erosion, and the growth of continental crust. *Reviews of Geophysics*, *29*(3), 279–316. https://doi.org/10.1029/91RG00969

Wadia, D. N. (1934). The Cambrian-Trias sequence of northwest Kashmir. *Records of the Geological Survey of India*, *68*, 121–176.

Wadia, D. N. (1937). Permo carboniferous limestone inliers in the Sub Himalayan Tertiary zone of Jammu, Kashmir Himalaya. *Records of the Geological Survey of India*, *72*, 162–173.

Walker, J., Martin, M., Bowring, S., Searle, M., Waters, D., & Hodges, K. (1999). Metamorphism, melting, and extension: Age constraints from the High Himalayan slab of southeast Zanskar and northwest Lahaul. *The Journal of Geology*, *107*(4), 473–495.

Wesnousky, S. G., Kumar, S., Mohindra, R., & Thakur, V. C. (1999). Uplift and convergence along the Himalayan Frontal thrust of India. *Tectonics*, *18*(6), 967–976. https://doi.org/10.1029/1999TC900026

Whipp, D., Ehlers, T., Blythe, A. E., & Burbank, D. (2007). Plio-Quaternary exhumation history of the central Nepalese Himalaya: 2. Thermokinematics model of thermochronometer exhumation. *Tectonics*, *26*, TC3003. https://doi.org/10.1029/2006TC001991

Whipple, K. X., & Meade, B. J. (2004). Controls on the strength of coupling among climate, erosion, and deformation in two-sided, frictional orogenic wedges at steady state. *Journal of Geophysical Research*, *109*, F01011. https://doi.org/10.1029/2003JF000019

Whipple, K. X., & Meade, B. J. (2006). Orogen response to changes in climatic and tectonic forcing. *Earth and Planetary Science Letters*, *243*(1-2), 218–228. https://doi.org/10.1016/j.epsl.2005.12.022

Whipple, K. X., & Tucker, G. E. (1999). Dynamics of the stream-power river incision model: Implications for height limits of mountain ranges, landscape response timescales, and research needs. *Journal of Geophysical Research*, *104*, 17,661–17,674.

Willett, S., Beaumont, C., & Fullsack, P. (1993). Mechanical model for the tectonics of doubly vergent compressional orogens. *Geology*, *21*(4), 371–374. https://doi.org/10.1130/0091-7613(1993)021<0371:MMFTTO>2.3.CO;2

Willett, S. D. (1999). Orogeny and orography: The effects of erosion on the structure of mountain belts. *Journal of Geophysical Research*, *104*(B12), 28,957–28,981. https://doi.org/10.1029/1999JB900248

Wobus, C., Heimsath, A., Whipple, K., & Hodges, K. (2005). Active out-of-sequence thrust faulting in the central Nepalese Himalaya. *Nature*, *434*(7036), 1008–1011. https://doi.org/10.1038/nature03499

Wobus, C., Hodges, K., & Whipple, K. (2003). Has focused denudation sustained active thrusting at the Himalayan topographic front? *Geology*, *31*(10), 861–864. https://doi.org/10.1130/G19730.1

Wobus, C. W., Whipple, K. X., & Hodges, K. V. (2006). Neotectonics of the central Nepalese Himalaya: Constraints from geomorphology, detrital 40Ar/39Ar thermochronology, and thermal modeling. *Tectonics*, *25*, TC4011. https://doi.org/10.1029/2005TC001935

Wolf, R. A., Farley, K. A., & Kass, D. M. (1998). Modeling of the temperature sensitivity of the apatite (U-Th)/He thermochronometer. *Chemical Geology*, *148*(1-2), 105–114. https://doi.org/10.1016/S0009-2541(98)00024-2

Yin, A. (2006). Cenozoic tectonic evolution of the Himalayan orogen as constrained by along-strike variation of structural geometry, exhumation history, and foreland sedimentation. *Earth-Science Reviews*, *76*(1-2), 1–131. https://doi.org/10.1016/j.earscirev.2005.05.004